MODELING AND VALIDATION OF PERCUSSIVE DRILLING PERFORMANCE IN A SIMULATED VISCO-ELASTO-PLASTIC ROCK MEDIUM

MAHMUD SHARIF SAZIDY

Modeling and Validation of Percussive Drilling Performance in a Simulated Visco-Elasto-Plastic Rock Medium

By

© Mahmud Sharif Sazidy

A thesis submitted to the School of Graduate Studies

in partial fulfillment of the requirement for the degree of

Master of Engineering

January, 2011

Faculty of Engineering and Applied Science

Memorial University of Newfoundland

St. John's, Newfoundland, Canada

ABSTRACT

Optimal force profiles are essential for extracting maximum performance from a percussion drilling system. In this investigation, a visco-elasto-plastic model of rock is simulated using the Bond Graph modeling technique to study the effect of different percussive force profiles on rock failure and to generate optimal force profiles. Physical parameters of the model are estimated from rock material properties like compressive strength, density, elastic modulus and Poisson's ratio using Hsieh's equations. The model predicts penetration due to crushing when applied force is greater than a threshold force of the rock medium. However, this model does not account for penetration due to rotary drilling bit shear or fluid flow. The simulated rock model is tested for three different strength rock formations.

A Specific Energy Index (SEI) and a Performance Index (PI) are employed to evaluate percussive force profiles. SEI reflects the effects of rate of penetration (ROP) and average hammer power where as PI considers rate of penetration, bit force, and input power. SEI is a limited metric because it recommends low frequencies and low rate of penetration. The Performance Index (PI) seems to strike a better compromise between ROP and power, and has the additional potential benefit of accounting for bit wear.

To validate the simulated model, rock physical parameters are tuned numerically by introducing a stiffness correction factor (K_s), a damping correction factor (K_b), and considering two different impact test scenarios. Published experimental results from the

TerraTek Single Cutter Impact Tester [22, 43-45] is used to verify four different rocks, and to study the effect of Bottomhole Mud Pressure (BHP) on penetration and damping correction factors. Another published experimental data from Drilling Research, Inc (DRI) implemented drop tests [48] on Indiana limestone is used to verify the model as well as to observe the change in damping correction factor with four different drop heights. Overall model validation results are in good agreement with the experimental data. However, further investigation is required to resolve many important issues and to characterize percussive drilling system.

The present visco-elasto-plastic rock model can be studied under both percussion and vibrational loading but here only percussive force profiles are analyzed. Follow up experimental work is ongoing, focused on characterization of different bit-rock type with the help of the developed rock model by measuring actual hammer force profiles and bit wear due to impact.

ACKNOWLEDGEMENT

First and foremost, all praise to God, the most gracious and merciful who gave me the opportunity and patience to carry out this research work.

I would like to express my sincerest gratitude to my academic supervisors, Dr. Stephen Butt and Dr. Geoff Rideout for their invaluable guidance, supervisions and constant encouragement throughout this research work. Working with them was a great learning experience and indeed without their assistance and support, this thesis would not have been completed.

Sincere thanks to our Project Manager, Farid Arvani for his valuable suggestions and help during this work. I also greatly appreciate the immeasurable co-operation and support from all the members of Advanced Drilling Group, Memorial University of Newfoundland.

This investigation has been funded by the Atlantic Innovation Fund (Contact no. 781-2636-192044), Industrial Research and Innovation Fund, Husky Energy and Suncor Energy. I am grateful to them for their financial support.

I would like to extend my gratitude to my parents, sisters and brothers for their inspiration and motivation in my higher study.

TABLE OF CONTENTS

LIST OF TABLES

LIST OF FIGURES

NOMENCLATURE

A_e	Bit effective contact area
b	Viscous damping coefficient
B_{avg}	Average force at bit
B_{pk}	Peak force at bit
C	Compressive strength of rock material
D	Threshold force of dry friction element
E	Elastic or Young modulus of rock
E_h	Energy of hammer
F	Applied normal force
$F_{BH}(t)$	Impact amplitude at BHP
F_f	Friction force
$F_G(t)$	Amplitude of generalized force profile
F_{slip}	Slip force
F_{spring}	Spring force
F_{stick}	Sticking force
$f_{1,2}$	Reissner's displacement functions
G	Shear modulus
g	Gap Between Blows

k	Spring stiffness
K_b	Damping Correction factor
K_f	Force scaling factor
Ks	Stiffness correction factor
M	Bit mass
M_r	Small mass of rock cuttings
P	Impact Amplitude
P_{avg}	Average hammer power
P_h	Hammer Power
R	Rate of penetration
r	Radius of effective contacts area
T_f	Impact fall time
T_r	Impact rise time
V	Volume of rock
$w_{1..,4}$	Weighting factors
x_1	Bit displacement
x_2	Penetration to rock
a_o	Dimensionless frequency
v	Poisson's ratio
ρ	Density of rock medium

Symbols and Elements Related to Bind Graph

C	Capacitive element
e	Efforts source
f	Flow source
I	Inductive element
p	Momentum
q	Displacement
R	Resistive elements
S_e	External effort source
V	Velocity

Abbreviation

BEM	Boundary Element Method
BHA	Bottom-Hole-Assembly
BHP	Bottomhole Mud Pressure
BOP	Blow-out-preventer
DRI	Drilling Research, Inc
DTH	Down-the-hole hammer
FEM	Finite Element Method
FDM	Finite Difference Method
F-P	Force-penetration

IF	Impact Amplitude product Frequency
MWD	Measurement while drilling
PI	Performance Index
ROP	Rate of Penetration
SEI	Specific Energy Index
TH	Top hammer
UCS	Uniaxial compressive test
WOB	Weight on bit

CHAPTER 1

INTRODUCTION

1.1 Introduction

It has been established and recognized that percussion drilling techniques drill faster than conventional rotary drilling in medium to hard rock formations. Highly operational risk, economical uncertainty and poor understanding of the mechanism limits this potential drilling technology for its wide application by the oil and gas industries.

The main goal of this present work is to develop a simulation tool to characterize percussive drilling performance by investigating the effect of different percussive force profiles on rate of penetration and energy requirement in hard rock drilling. Rock medium

has been modeled as a visco-elasto-plastic material using lumped parameter elements to predict rate of penetration (ROP) under vibro-impact or percussive loading.

The lumped parameter rock model is validated and tuned using a single impact test on different rock formations [22, 43-45], and a simple drop test on Indiana limestone [48].

This chapter will give a general introduction of different drilling methods, important drilling components and systems, a brief comparative study between conventional rotary drilling and percussion drilling, and finally presents an outline of the whole research work.

1.2 Drilling Methods

Drilling is a process of material removal to produce a ground hole or well. This process is widely used in oil, gas, geothermal, minerals, water wells, and mining industries. A drilling operation needs to perform the following six basic functions to produce a hole [35],

- Transformation of energy to the bit-rock interface
- Reduction of the rock
- Removal of the rock
- Maintenance of the borehole (formation stability) while drilling
- Control of formation fluids (well control)
- Preservation of the borehole (completion)

In the last 50 years, approximately ten drilling methods have been investigated to reduce drilling cost and improve overall performance. Mechanical drilling method is the most widely used and efficient method over laser drilling, chemical drilling and electrical drilling methods. The mechanical drilling process has two basic forms, conventional rotary action and percussive action. Figure 1.1 gives a schematic diagram of conventional rotary drilling. In general, conventional rotary drilling involves different rig systems such as power generation system, hoisting system, fluid circulation system, rotary system, well control system, data acquisition and monitoring system.

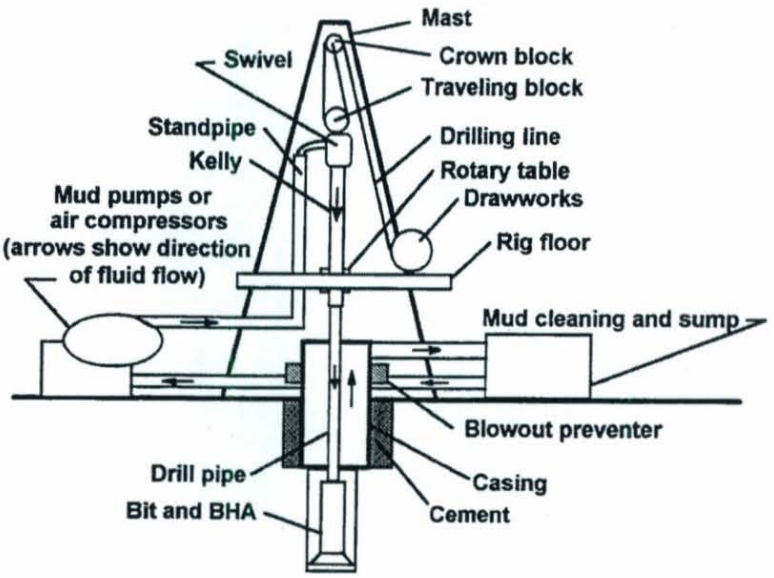

Figure 1.1 Schematic of a conventional rotary drilling process [35]

A rotary percussion drilling requires an additional impact tool to generate percussive force, whereas in percussive mode of drilling operation, no rotary system exists other than a blow indexing mechanism [28].

1.3 Drilling System Components

All the necessary components for a drilling operation are organized under a derrick or mast. Drill collar, drill pipe and drill bit are the main functional components of a drilling system. The drill pipe acts as a prime mover to convert energy from a diesel-electrical driven power generation system into mechanical energy, which is transmitted through drill collar, drill bit and other drill string components to the rock surface. A drill string is composed of drill pipe and Bottom-hole-assembly (BHA). A BHA consists of drill collars, drill bit, stabilizers and some special tools below the drill pipe. The drill collar provides effective weight on bit (WOB) or thrust into the bit, and the bit hits the rock surface to generate penetration.

The main components of a hoisting system in a drilling system are, draw works, crown block, traveling block, drilling line and elevator. The principal function of a hoisting system is to hoist the drill string.

The primary function of a fluid circulation system is to remove cuttings from bottom hole surface and to act as a cooling fluid for drill string components by circulating a drilling fluid or mud from the surface to the bottom hole and back to the surface again. A fluid circulating system is composed of a mud pump, high-pressure surface connectors, drill string, return annulus, mud pit and mud treatment equipment.

In a rotary system, drill pipe, drill collar, swivel, rotary table and kelly are inset into the drill rig floor to achieve drill bit rotation. Some of the drill rigs use a top-drive motor instead of rotary table to give bit rotation. In directional well drilling, down hole motors are widely used to rotate the bit. A rotary percussion system has an additional tool, either a top hammer or a down-the-hole hammer to generate short duration impact impulse. For a simple percussion drilling system, a blow indexing mechanism gives slow rotation to the bit instead of a rotary system.

A well control system is of primary importance in any drilling system for its safe and smooth operation, to prevent flow of formation fluid into the well bore during a kick with the help of blow-out-preventer (BOP). A typical BOP is shown in Figure 1.2, which consists of annular preventer, ram preventer, spools, internal preventer, casing head, flow lines, choke lines, kill line-connectors, mud-gas handling facilities and accumulators.

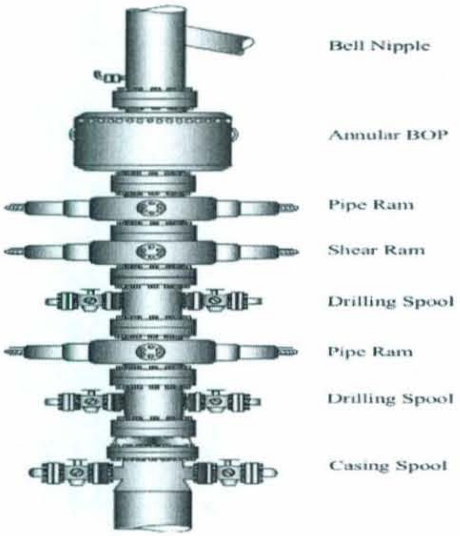

Figure 1.2 A typical Blow-out-preventer stack [52]

The data acquisition and monitoring system are used to monitor, record, analyze different drilling related parameters like penetration rate, pump pressure, fluid flow rate, torque, rotary speed, WOB , mud density etc.

There is a wide variety of drill bits used in operation, which strike the rock surface to crush and break it. Figure 1.3 shows three different types of drill bits commonly used in drilling fields. The roller-cone bit crushes the rock by turning its cones and teeth successively when it comes in contact with fresh rock surface, whereas a drag bit cuts the rock material by its shearing action. Drag bits are widely used in soft to medium rock formations for their faster drilling rate and long life. In percussion drilling, either conventional roller cone bits or solid-head bits with tungsten-carbide inserts can be used for hard rock formations.

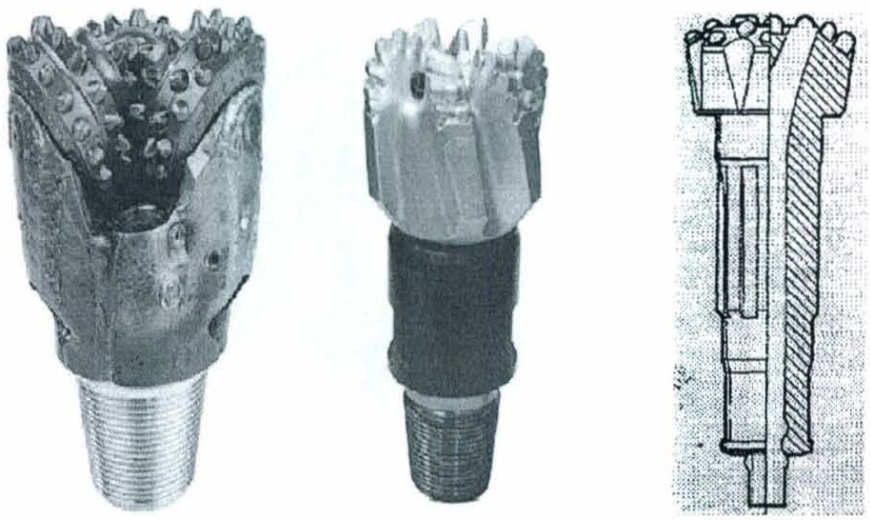

Roller-Cone bit **Drag bit (PDC cutters)** **Solid-head bit**

Figure 1.3 Commonly used drill bit type [35, 52]

1.4 Percussive Drilling System

Percussion drilling is one of the most classic drilling mechanisms for hard rock formations. An impact tool or piston in a percussion hammer generates short duration impact stress waves which are transmitted to the rock in order to cause failure of the material. In percussion drilling, a piston driven by compressed air or hydraulic drilling mud converts its kinetic energy to impact energy by colliding with a steel rod or drill bit. This impact energy is transferred to the steel in the form of a stress wave that travels to the bit rock interface. Part of the energy in the wave goes to the rock, causing failure, and part of the energy is reflected back. The effective stress in breaking rock acts in an axial direction and in a pulsating manner [28]. Rock failure due to this impact stress wave is an important phenomenon which needs to be considered in percussion drilling, which will be discussed later in more detail. A thrust load or WOB is applied to the drill bit string to maintain intimate contact between drill bit and rock surface. Unlike conventional rotary system, percussion drilling system has a blow indexing mechanism which provides a small rotation to the bit; and hence impacts are produced on the rock in different positions.

Percussion drilling methods are classified into two groups based on hammer position in the system. In top hammer (TH) percussion drilling, the hammer is located at the top of the drill string and transmits energy to the bit through the drill steel, whereas in down-the-hole hammer (DTH) drilling, the hammer is positioned just above the bit and it directly

strikes the bit to generate impulsive force. Figure 1.4 indicates basic difference between these two types of percussive drilling mechanisms.

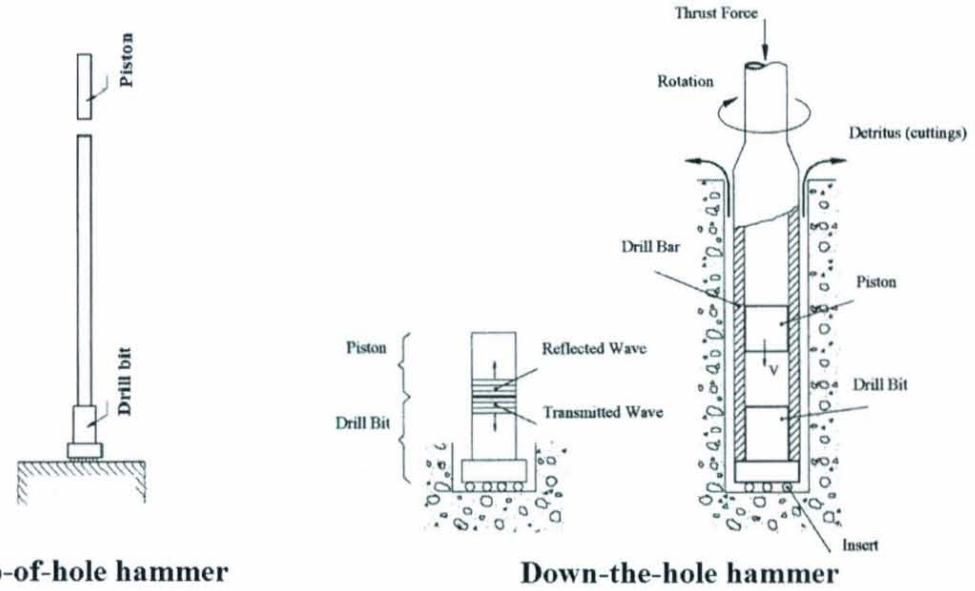

Figure 1.4 Basic principles of TH and DTH [15]

1.5 Research Objectives and Approaches

The current investigation is a part of research project entitled "Advanced Drilling Technology" [36]. The objective of this research work is to develop a simulation tool that helps to understand percussion drilling and other types of vibration assisted drilling mechanisms.

Therefore, a rock model is developed assuming a visco-elasto-plastic material to select an optimal percussive hammer force profile by analyzing the model under percussive loading. Physical parameters of the model are estimated from rock material properties

like compressive strength, density, elastic modulus and Poisson's ratio using Hsieh's equation [32]. Two drilling performance matrices are employed to evaluate percussive drilling performance.

The rock model has been validated by using experimental data obtained from two different types of impact test sources [22, 43-45, 48].

The whole investigation has been divided into six chapters. The first chapter addresses the general background, objectives and the scope of the proposed research work. A detailed outline of the research work is listed below and is shown in Figure 1.5.

Chapter 2 involves a brief review of currently available drilling technologies, particularly percussion drilling technology in petroleum industries, rock failure mechanism under dynamic loading or vibro-impact loading, numerical and experimental studies of percussion drilling, drilling parameter optimization and limitation of some of the previous work related to percussion drilling.

Chapter 3 gives a brief introduction of bond graph modeling, modeling of rock as a visco-elasto-plastic material, and derivation of system equation from the bond graph in their differential explicit form. This chapter introduces a simple methodology to estimate physical parameters of the model using common rock material properties. This chapter also involves formulation of Specific Energy Index (SEI) and a new performance Index (PI) to evaluate performance of tools with different force profiles.

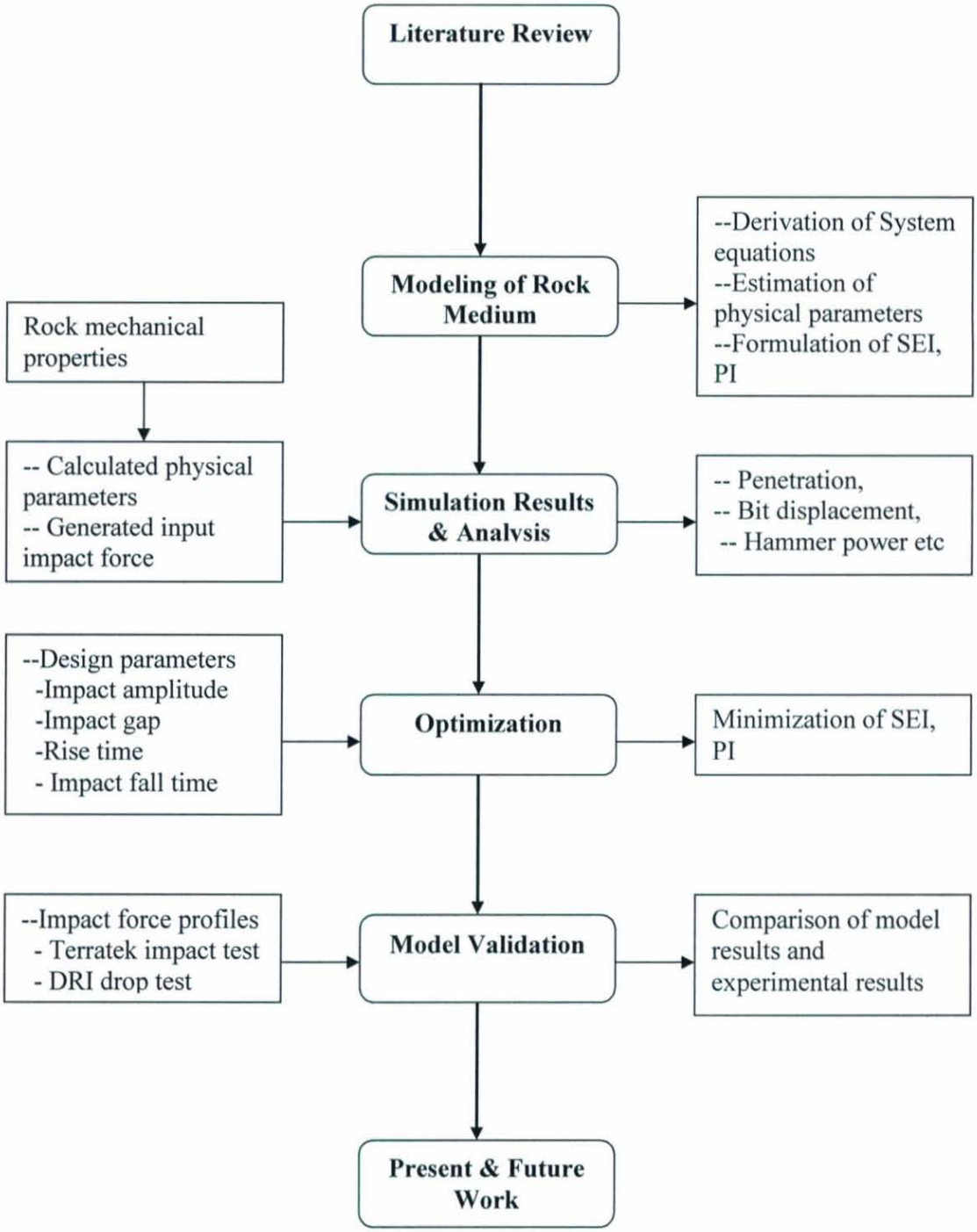

Figure 1.5 Flow chart of present research work.

Chapter 4 demonstrates the performance test of the simulated rock model under simple percussion as well as in three different rock formations. Different percussive force profiles are analyzed over a range of design parameters and the performance matrices are used to determine optimal force profile.

Chapter 5 shows the model validation and calibration process using TerraTek [22, 43-45] and Drilling Research, Inc (DRI) [48] conducted single impact test results. It also involves the study of the effect of bottomhole pressure (BHP) on different performance parameters.

Chapter 8 summarizes and concludes the findings and limitations of the present work. This chapter also includes original contributions of this thesis along with some guide lines for future work.

CHAPTER 2

LITERATURE REVIEW

2.1 Introduction

It is advantageous from an economic and strategic point of view to develop new drilling tools to improve rate of penetration and overall drilling efficiency for challenging formations such as hard rocks. Drilling industries and researchers have directed their investigation towards different novel and new drilling technologies to overcome these challenges so that improved drilling performance and reduction in drilling cost can be achieved. Previous research has established than percussive drilling techniques drill much faster that conventional drilling in hard rock structures [1-4, 22, 28].

Han et al. [2] describe the history of percussive drilling, first developed by the Chinese about 4000 years ago. At that time it often took two to three generations of workers to complete large wells. The first oil well using a cable tool percussion machine was completed by Drake in 1859. A great contribution was found from researchers in the 1900's for a huge increment in penetration rate from 3-5 m/hr to 450 m/hr [sic] for an underground small percussion blast tool [37].

Major developments and research works were carried out in the 1950's and 1960's. Since then different terms have been used such as down-the-hole hammer (DTH), top hammer (TH), percussion hammer, rotary percussion drilling etc. Unfortunately, wide application of percussion drilling was not noticed to the oil and gas industry until 1980's. Since 1980 percussive drilling attracts industries because of its high efficiency and flexibility in hard rock formations.

In early 1970's, significant research and investigation on percussion drilling was done by W. A. Hustrulid and C. Fairhurst [1, 6, 7, 34]. Their efforts on percussion drilling can be best described as the pioneering of work on the theoretical and experimental study of the percussion drilling of rock for energy transfer, drill steel-piston interface, thrust force requirements and indexing mechanism. In recent times TerraTek has been conducting several analytical and experimental investigations on percussive drilling, which can be seen in publications by Green et al. [22], Han et al. [2, 4, 43-45].

The following sections of this chapter will discuss typical response of rock medium to percussive or impact loading, modeling efforts by different researchers, popular drilling operation optimization techniques, experimental investigation on percussion drilling, and current status of percussion drilling.

2.2 Rock Behavior Under Percussion

Rock response to dynamic loading is drastically different from its response to static loading because of its extremely complex nature. Therefore, it is very important to clearly understand the rock behavior and physics involved in rock failure when the rocks are subjected to different dynamic loading conditions. This may facilitate development of simulation tools to better characterize the percussion drilling system.

Rock behavior and breaking criteria have been studied and described by many researchers. W. C. Maurer [53] defines the percussion drilling system, in which the drill bit applies force perpendicular to the rock surface and the bit moves into the rock perpendicular to the surface and in a direction of applied force, following a crater beneath it.

According to Han et al. [44], there are four fundamental processes in percussion drilling as shown in Figure 2.1 to complete a drilling operation. The physics involved in the entire

percussive drilling process was also described by W.C. Maurer [53], Hustrulid et al. [1] and many other authors.

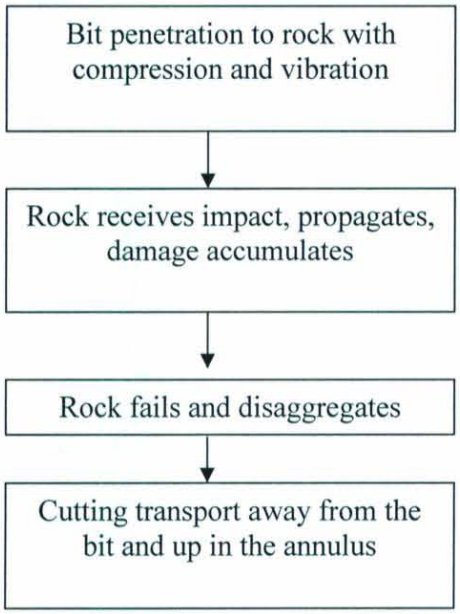

Figure 2.1 Basic fundamental processes in percussion drilling [44]

Hustrulid et al. [1] and later on many authors developed the theory of percussion drilling and explained it based on stress wave propagation theory. Hustrulid et al [1] and Chiang et al [15] explained the stress wave generated by the impact of hammer piston and drill bit which travels to the bit-rock interface. From this incoming stress wave, most of the energy is utilized in rock breaking, and a fraction of it is reflected by the rock surface. Hustrulid et al. [1] also mentioned that the energy transfer to the rock occurs from the first two incident waves only.

The fundamental of rock failure process due to percussive type loading has been best explained by W. C. Maurer [53], and it can be shown in Figure 2.2.

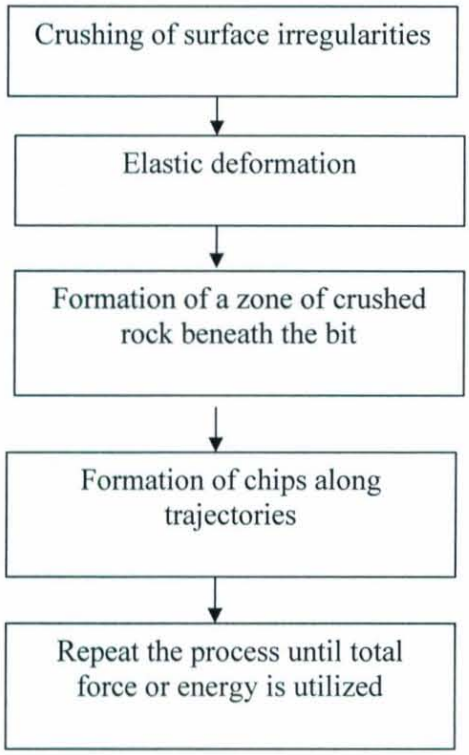

Figure 2.2 Rock failure process in percussion drilling [53]

A broad overview is found in Han et al. [2, 4, 43] on rock failure mechanisms under both conventional rotary drilling and percussion drilling conditions. The basic differences between these two drilling methods in terms of rock defragmentation are shown in Figure 2.3.

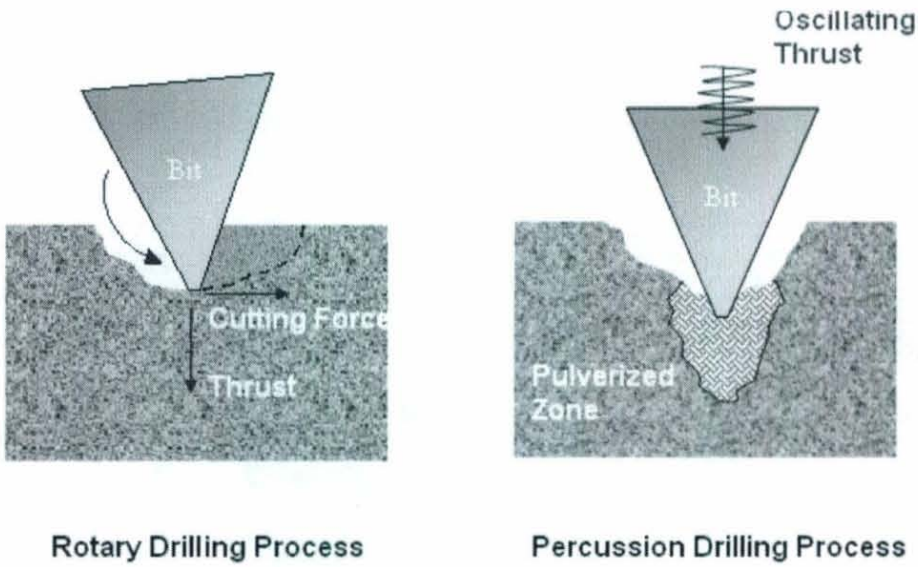

Figure 2.3 Rock failure process in rotary and percussion drilling [2]

From Figure 2.3, it is noticeable that in conventional rotary drilling the rock fails because of axial thrust (WOB) and drill bit rotation. The bit penetrates rock in the axial direction due to WOB and then shears a conchoidal chip because of bit rotation. In percussion drilling a hammer tool produces a short duration high amplitude impact force along the direction of bit movement. When this impact force exceeds the compressive strength of the rock medium, it crushes the rock below the bit and creates fractures forming a narrow wedge along the outer boundaries of the bit inserts [4].

2.3 Modeling Efforts in Percussion Drilling

Nowadays, many researchers focused their investigation towards modeling of percussion drilling systems and developing simulation tools to better characterize this promising drilling technology.

L. E. Chiang and D. A. Elias [15] developed a numerical method based on the impulse momentum principle to use as a design tool for pneumatic DTH hammers to predict the effect of mass distribution, boundary conditions, geometry, and the type of rock on the stress wave transmission efficiency. Similar to Chiang's [12] work, they have considered the rock medium as a non-linear spring attached to the drill bit end which follows a force-displacement law for a particular rock-bit combination. L. E. Chiang and D. A. Elias [13] in another publication presented a three dimensional (3D) finite element model of impact in rock drilling in order to simulate energy transmission to the rock, the bit-rock interaction, and the process of rock fragmentation. Their analytical and experimental investigation simplified the simulation of impact tool and helped to obtain various hammer performance information, which is necessary for the hammer design purpose. In their study some of the important factors such as rock fracture, air flushing speed, rotation speed, etc. is not considered which might have strong effect on penetration. Their theoretical results are in good agreement with experimental data. However, the model still cannot accurately predict the penetration, yet it very much helpful when comparing two different hammers same as the present rock model.

Han et al [2, 4, 43, 44] introduced a 3D dynamic model of hard rock to investigate percussion drilling and proposed three failure criteria: critical compressive strain criteria, critical shear plastic strain criteria and tensile failure criteria. They have tested elastic, Mohr-Coulomb and strain softening models. Plot of failure advancement, rock failure history and rock fatigue/ damage history from their simulation model answers why, how and when the rock fails. This information is important for the theoretical analysis of percussion tool, and further the information was helpful in modeling present visco-elasto-plastic rock model.

Izquierdo et al. [14] created two simulation models of DTH hammers. Their thermodynamic model of DTH hammer helps in determining piston kinetic energy at impact, impact velocity and impact frequency whereas a stress wave propagation model was used to estimate energy delivered to the rock. Lundberg et al. [16] presented two different rock models under impact loading. The first model was perfectly rigid, represented by an inelastic spring, and the second model was linearly elastic with a linear spring. None of these models considered the damping effect of rock medium.

Damping is an important factor in determining the efficiency of percussion drilling. Han et al. [4] showed the effect of damping on stress wave propagation and recommended appropriate damping features to achieve simulation results that can closely match with the rock behavior. Apple et al. [39] considered damping effect in their rock model, and

simulated rock behavior as an equivalent lumped system to investigate chisel-bit penetration on rock as shown in Figure 2.4.

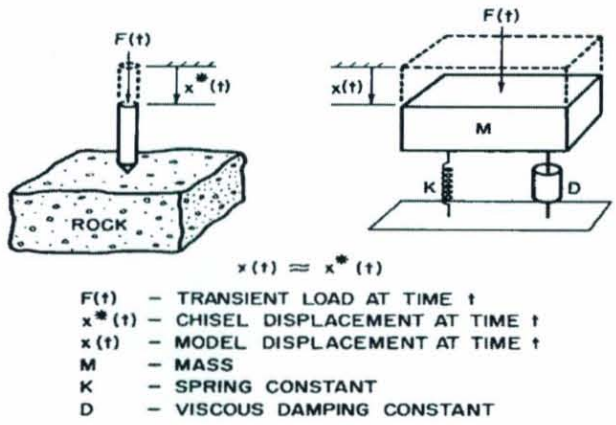

Figure 2.4 Equivalent lumped parameter model of rock [39]

The rock model in Figure 2.4 has three parameters: effective mass, spring constant and a damping constant to represent the rock model under dynamic loading. They showed a methodology to calculate effective mass and spring constant to match model penetration with actual chisel penetration. Unfortunately, they found difficulties in calculating viscous damping constant and for the entire analysis this parameter was set to zero.

Pavaloski et al. [17] modeled the rock as a visco-elastic material whereas Fernando et al. [19] introduced a non-linear spring–dashpot system. Both of the mechanisms allow visco-elastic force to overcome friction force or resistance force of the media and enables bit penetration in to the rock. A similar but slightly different rock model was presented by Batako et al. [20], where the rock medium is considered as visco-elasto-plastic material.

They introduced stick-slip phenomenon to generate an impact action which applied to the drilling process.

2.4 Performance Evaluation and Optimization

It is well known that rate of drilling penetration is the most important performance parameter for drilling performance evaluation especially when two hammers or two force profiles are compared. However, other performance parameters like power consumption and bit wear should also be considered to select the optimum percussive force profile. To date, several methods and criteria are available and commonly followed by industries and researchers to evaluate the drilling performance. Kennedy et al. [28] introduced performance criteria based on energy, power, ROP, bit wear and some cost functions for use under particular field circumstances. Wilson et al. [25], Iqbal et al. [26] demonstrated a cost function for optimization purposes by considering WOB and rotary speed as controlled parameters for rotary drilling. Izquierdo [14] formulated a Specific Rock Energy Index which is a function of hammer power, ROP, thrust force, torque and angular velocity. Hustrulid et al. [6] used depth per blow, volume per unit energy or specific energy for some of their hammer performance analysis. Topanelian et al. [11] introduced a new factor known as IF factor, the product of impact amplitude and impact frequency to study the performance of different percussion hammers.

In this investigation, two methods of performance analysis are used: the Specific Energy Index (SEI) similar to that of Izquierdo et al. [14], and a proposed Performance Index (PI) based on ROP, average hammer power, maximum bit force and average bit force. For this

new PI, weighting factors are chosen to assign relative importance of these parameters. This PI has potential advantages over above mentioned performance criteria's which will be discussed more detail in Chapter 4.

2.5 Experimental Investigation of Percussion Drilling

Most of the experimental works on percussion drilling are limited to small scale laboratory tests, and the primary reasons for these tests are to generate force-penetration (F-P) curves, investigate actual percussion hammer force profiles, and determine crater volume, energy requirement etc. Experimentally obtained F-P curve are considered as invaluable tool for calibrating and validating theoretically developed rock models.

Single cutter impact tests or simple drop tests are the most common types of experimental work used to investigate percussive drilling. It is found that most of the impact test apparatus are simple in their mechanical design but rather complicated in instrumentation and measurement process. Therefore, the review in this section will focus on experimental system developed as well as instruments used for the force and penetration measurement by different researchers.

W. A. Hustrulid and C. Fairhurst conducted several series of experiment with their drop tester [6] and long-rod apparatus [7] to verify their theoretical analysis. In their drop tester, a winged bit attached to a mass block was allowed to free fall on the rock surface through three guide rods in order to determine F-P relation and energy per unit crater

volume from different drop height. A special Plexiglas ring and putty was used to measure the volume of missing material. The information of average volume of missing material and average cross-sectional area were used to obtain penetration depth in the rock. Two strain gauges were mounted on the shank to get force-time histories. In the long-rod apparatus, a 10 ft long steel rod which can move vertically by two ball-bearing mounted guides, and an electromagnet was used to release the piston to impacts on the drill steel. A carbide inserts bit was attached to the bottom of the steel rod and held against rock specimen. In the long-rod apparatus, bit force, bit displacement, reflected stress waveforms were measured, and corresponded to their predicted results on the basis of observed experimental results for different bit-rock types. Strain gauges were installed on the steel rod at three different locations. The shank gauges were used to record the incident wave and the time of piston-drill steel separation whereas middle gauges were used to record incident and reflected strain wave, and strain gauges at the bit were used to obtain force-time record at the bit-rock interface.

Apple et al. [39] developed an experimental rock-chipper mechanism apparatus to validate their previously discussed rock model. The rock-chipper apparatus generated single blows with an electromagnetic clutch and brake-cam mechanism. The test was performed on Bedford limestone and Beekmantown dolomite. The force-time series was recorded by strain gauges mounted on the chisel shank whereas the displacement was measured by integrating velocity data obtained from a velocity transducer mounted between the chisel shank and rock surface. They found a good agreement between their

theoretical and experimental results. However, the frequency range of the experiment was limited to 240cycles/sec only.

Topanelian [11] conducted an experiment to study the effect of low frequency percussion in granite rock block. A hydraulically lifted rotary table was used to rotate and to force the test block upward. Tubular hammers of different weights were lifted mechanically and allowed to drop by gravity from various heights onto a floating anvil to obtain percussion force. Impact force and kinetic energy of the hammer was determined from load cell attached to the bottom of the anvil.

L.E. Chiang [12] developed a simple experimental system to obtain dynamic F-P curves for validating their momentum-impulse based simulated signal, in which a hand held steel hammer strikes a steel slender chisel bit held against the rock specimen. Two strain gauges were placed on the chisel to measure force and the actual displacement was found from an optical displacement transducer.

An extensive experimental work was carried out by Yang et al. [41] and Padio et al [40] with single-blow bit-tooth impact tests on saturated rock under confining pressure considering both zero pore pressure and rising pore pressure. The basic measurement involved force-time, displacement-time, velocity-time, and from them generation of F-P curves during crater formation. Their investigation was targeted to find out the failure mode of rock under different pore fluid pressures for a constant bit tooth geometry,

penetration and impact velocity during the single impact test. Pore pressure and BHP was controlled separately by a confining pressure and pore pressure system.

Hartman [42] employed an impact device or drop tester, in which a chisel shaped bit was attached to a plate which can freely fall by gravity on the rock through two guide rods. The main objective was to simulate percussive drilling by studying the effect of blow indexing on drilling performances considering both fresh and damaged rock surface.

DRI also demonstrated a drop test experiment to study the relation of energy, velocity and momentum of the percussive blow to the amount of rock drilling [48]. In recent times, considerable experiments have been done by Green et al. [22] and Han et al. [2, 4, 43-45] using the TerraTek single cutter impact tester. Both the DRI implemented drop tester and TerraTek single cutter impact tester are discussed in detail in Chapter 5. Some of their experimental data were used to validate the present simulated visco-elasto-plastic rock model.

2.6 Current Status of Percussion Drilling

Recent progress and achievement in percussion drilling encourages oil and gas industries to pay attention to this potential technology in order to improve drilling performance especially for hard rocks. In the last 50 years, significant efforts were directed by the researchers in numerical modeling based on Finite Element Method (FEM), Boundary

Element Method (BEM), Finite Difference Method (FDM), rock block theory, application of different analysis methods etc.

Many authors reported the successful application of percussive drilling technology in the laboratory as well as field operations, and its potential outcome and benefits over conventional rotary drilling. Han et al. [4] mentioned percussive drilling with combined rotary action producing 7.3 times faster penetration than conventional drilling at a given WOB and rotary speed. However, negative factors associated with this technology limit its wide application and acceptance by the industries. Pierce et al. [35] listed some of the negative features of a mud hammer used in percussion drilling

- Performance improvement decreases with depth
- Hammer designs which valve the total mud flow are a hindrance to well control operations
- Hammer interfaces with mud-pulse or acoustic MWD
- Poor design or incorrect operation can causes excessive damage at the hammer-anvil interface
- Abrasives in mud causes erosion and wear at the control valve
- Fatigue may cause mechanical failure of the valve and/or spring

According to Han et al. [2, 4, 43-45], there are four main key obstacles to percussion drilling that need to be overcome,

1. Lack of fundamental understanding of rock mechanics

2. Risks associated with the operation
3. Economical uncertainties
4. There are no or very few simulation tools available to help design and optimization of this drilling system.

Another important concern is the validation of percussion model. Significant challenges are associated with validating or calibrating models, mainly because of unavailability of field operational data or experimental data. These negative factors need to be overcome for the development of more efficient technology, and to be more acceptable to the oil and gas industry.

CHAPTER 3

MODELING AND SYSTEM EQUATIONS

3.1 Introduction

In an attempt to analyze percussive and other vibro-impact force profiles, the work described in this chapter simulates a visco-elasto-plastic rock model similar to Batako et al. [20] with 20*sim* bond graph based software [30]. The software is used to generate different percussive and vibrational force profiles that closely match with real percussive or vibro-impact tool motion profiles. Stiffness and damping coefficient of the model rock are computed using Hsieh's equations [32] which are based on elastic half-space theory. Two methods of performance analysis are introduced: the Specific Energy Index (SEI) similar to that of Izquierdo et al. [14], and a proposed Performance Index (PI) based on ROP, average hammer power, maximum bit force and average bit force.

3.2 Rock Failure Under Vibro-impact Loading

Rock behavior under impact loading exhibits complex behavior. Chiang et al. [13] indicated that hard rocks deform linearly until breakage, which often occurs in a violent and sudden way, whereas soft rocks do not show this linearity or sudden failure. These are indicated by the typical stress-strain curves of hard and soft rock shown in Figure 3.1.

Percussive drilling techniques show good performance in hard rock formations like sandstone, limestone, granite etc. and hence a visco-elasto-plastic model of rock similar to Batako et al. [20] is considered in this study.

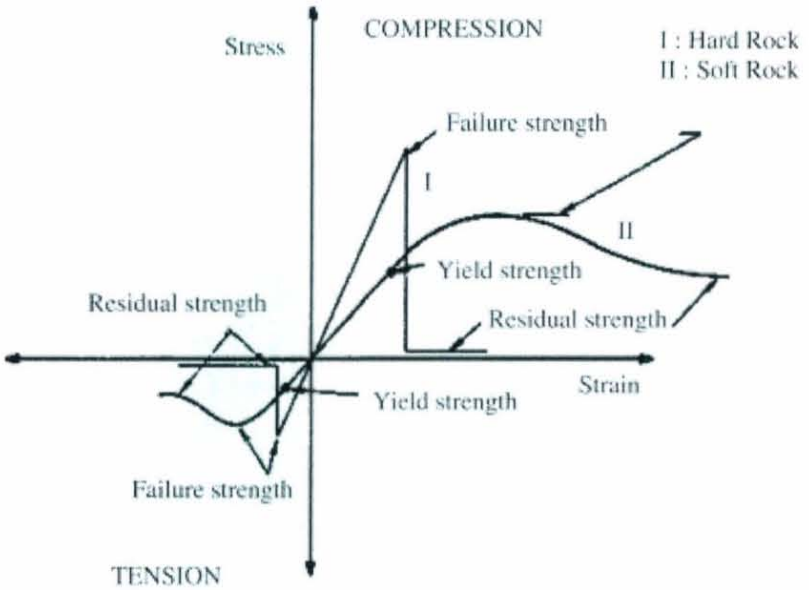

Figure 3.1 Stress-strain curve of hard rock and soft rock [13]

A visco-elasto-plastic model of rock is shown in Figure 3.2. The rock model consists of a bit mass (m), linear stiffness (k), viscous damping coefficient (b) and dry friction element

with a threshold force of D. The stiffness and damping coefficients represent the visco-elastic nature of hard rock before failure and the dry friction element (D) is the crushing force threshold of the rock medium. The small mass of rock cuttings (M_r) shown in Figure 3.2 has negligible effect on the simulation results but acts as a parasitic mass element to allow an explicit set of ordinary differential equations to be written.

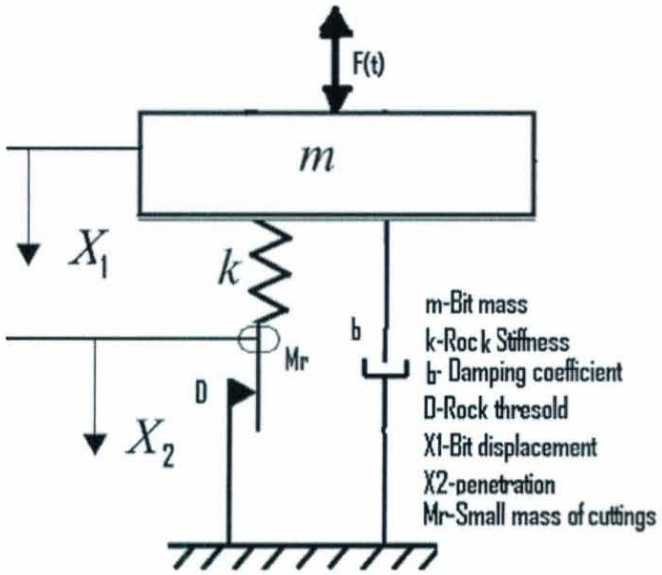

Figure 3.2 Diagram of visco-elasto-plastic rock model

When a normal force (F) is applied to the bit, spring force (F_{spring}) builds up in the visco-elastic zone but no penetration movement of bit (X_2) is achieved as long as spring force (F_{spring}) does not exceed the rock threshold force. When the spring force exceeds the threshold, the rock fails and the dry friction element moves to simulate the rock deforming plastically. During this plastic deformation of rock, it is assumed that all cuttings are removed instantly from the crushed surface.

3.3 Bond Graph Background

Bond graphs are a graphical modeling language (examples of other graphical modeling languages are block diagrams and signal-flow diagrams) in which mechanical, electrical, thermofluid, and magnetic systems are represented with a small set of generalized energy storage, dissipation and transfer elements. Elements are connected with power bonds, each of which contains a pair of signals generally known as "effort" and "flow" whose product gives instantaneous power of the bond. For an electrical system, effort and flow are voltage and current respectively, and for a mechanical system they are force and velocity. Half arrows on the bonds define the direction of positive power flow, and control signals are represented by lines with full arrows. Casual strokes, placed normal to one end of each bond, define whether or not an element has a causal flow or effort output when assembling system equations. Generalized Kirchhoff loops and nodes are represented by 0- and 1-junctions. Elements bonded to a 0-junction have common effort, and their flows algebraically sum to zero. Elements bonded to a 1-junction have common flow but the algebraic sum of their efforts is zero. Bond graphs facilitate the generation of governing equations, allow prediction of numerical issues such as implicit and differential-algebraic equations, and allow easy combination of electrical, mechanical and thermo-fluid submodels. For more details about bond graph modeling see Karnopp et al. [27].

Figure 3.3 is the simplified bond graph drawn from the diagram of the visco-elasto-plastic model of rock under vibro-impact loading shown in Figure 3.2. The diagram is composed of 1-junctions, 0-junctions, external effort source (Se) for force input, capacitive element

(*C*) for the spring, resistive elements (*R*) for the dry and viscous friction elements, and a generalized inductive element (*I*) for the bit and parasitic mass. Typically, state variables in the bond graph formalism are generalized momentum (*p*) and displacement (*q*).

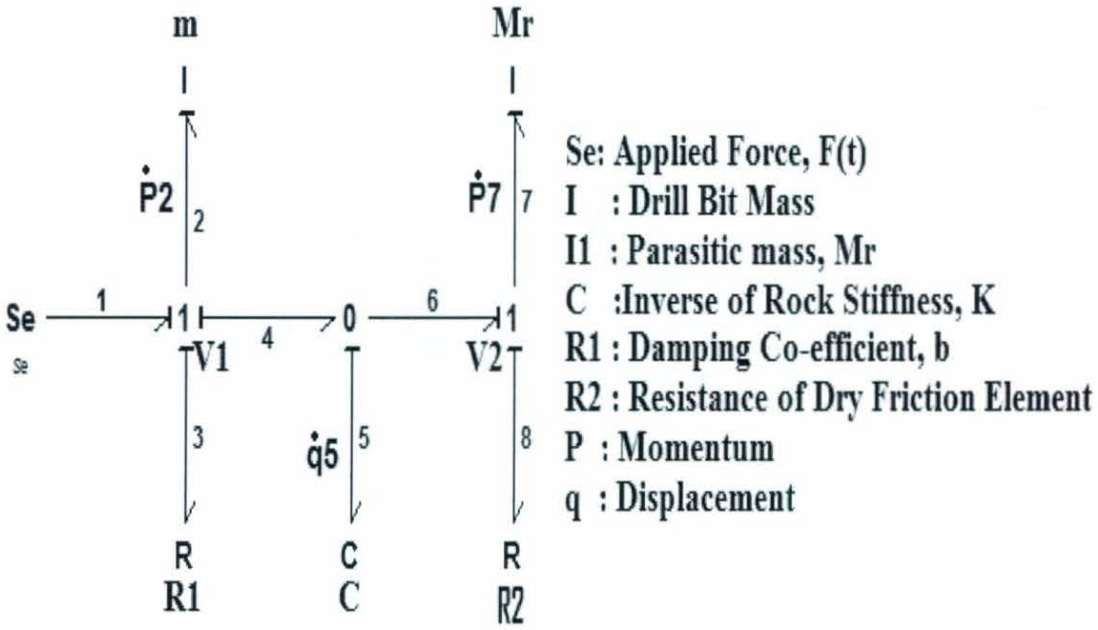

Figure 3.3 Bond graph model of visco-elasto-plastic rock medium under impact loading

3.4 Derivation of System Equations

A set of explicit ordinary differential equations will now be derived from the bond graph shown in Figure 3.3.

$$\overline{X} = \begin{bmatrix} p_2 \\ p_7 \\ q_5 \end{bmatrix}$$

where p_2 and p_7 are the momentum of the bit and cuttings masses, and q_5 is the spring displacement.

At the V_1 velocity 1-junction summation of efforts (e) are zero but all flows (f) are equal. Hence

$\sum e = 0$ and $f_2 = f_3$;

$$\Rightarrow e_1 - e_2 - e_3 - e_4 = 0 \tag{3.1}$$

Now, $e_1 = Se$ = input force $F(t)$, $e_2 = \dot{p}_2$, $e_3 = f_3 R_1$ and $e_4 = e_5$. So, Eq. (3.1) becomes

$$\Rightarrow Se - \dot{p}_2 - f_3 R_1 - e_5 = 0$$

Also, $f_3 = f_2$, $e_5 = \frac{q_5}{C}$ and $f_2 = \frac{p_2}{m}$. So,

$$\dot{p}_2 = Se - \frac{p_2}{m} R_1 - \frac{q_5}{C} \tag{3.2}$$

At the V_2 1-junction,

$$\dot{p}_7 = e_6 - e_8 \tag{3.3}$$

Substitute, $e_6 = e_5 = \frac{q_5}{C}$ and $e_8 = F_f$, where F_f is the dry friction force of rock medium.

Hence,

$$\dot{p}_7 = \frac{q_5}{C} - F_f \tag{3.4}$$

At the 0-junction,

$$\dot{q}_5 = f_4 - f_5$$

$$\Rightarrow \dot{q}_5 = f_2 - f_7$$

$$\Rightarrow \dot{q}_5 = \frac{p_2}{m} - \frac{p_7}{M_r} \tag{3.5}$$

Eq. (3.2), (3.4), (3.5) are the state equations of the model and can be written as,

$$\begin{bmatrix} \dot{p}_2 \\ \dot{p}_7 \\ \dot{q}_5 \end{bmatrix} = \begin{bmatrix} -\frac{R_1}{m} & 0 & -\frac{1}{C} \\ 0 & 0 & \frac{1}{C} \\ \frac{1}{m} & 0 & -\frac{1}{M_r} \end{bmatrix} \begin{bmatrix} p_2 \\ p_7 \\ q_5 \end{bmatrix} + \begin{bmatrix} 1 \\ 0 \\ 0 \end{bmatrix} [Se] + \begin{bmatrix} 0 \\ -1 \\ 0 \end{bmatrix} [F_f] \tag{3.6}$$

Substitute, $R_1 = b$, $C = \frac{1}{k}$ and $Se = F(t)$

$$\begin{bmatrix} \dot{p}_2 \\ \dot{p}_7 \\ \dot{q}_5 \end{bmatrix} = \begin{bmatrix} -\frac{b}{m} & 0 & -k \\ 0 & 0 & k \\ \frac{1}{m} & 0 & -\frac{1}{M_r} \end{bmatrix} \begin{bmatrix} p_2 \\ p_7 \\ q_5 \end{bmatrix} + \begin{bmatrix} 1 \\ 0 \\ 0 \end{bmatrix} [F(t)] + \begin{bmatrix} 0 \\ -1 \\ 0 \end{bmatrix} [F_f] \tag{3.7}$$

Eq. (3.7) is the generalized form of state equations for the system. To simulate and study the system response in the visco-elastic phase and the plastic phase, Karnopp's [29] stick-slip friction modeling approach is utilized in which the dry friction element "locks" when the velocity (V_2) enters a region of small non-zero velocity defined as $-DV < V_2 < DV$. Karnopp used the small velocity region instead of exact zero velocity as the locking criterion in order to reduce numerical simulation issues inherent to discontinuous systems.

Case-I: In the visco-elastic region or sticking region, velocity of the dry friction element falls inside the small-velocity region and is assigned a zero value. Total friction force (F_f) is the sticking force (F_{stick}) of this region and its value is limited by threshold force D. F_{stick} is equal to the spring force developed by the elastic element in series with the dry friction element. Sticking force can be calculated as follows,

$$\dot{p}_7 = F_{Spring} - F_f \text{ and } V_2 = \frac{p_7}{M_r}$$

As V_2 tends to zero, p_7 also tends to zero. So,

$F_f = F_{stick} = F_{spring} = \frac{q_5}{C} = kq_5$, and the state equations for the visco-elasic region are,

$$\begin{bmatrix} \dot{p}_2 \\ \dot{q}_5 \end{bmatrix} = \begin{bmatrix} -\frac{b}{m} & -k \\ \frac{1}{m} & 0 \end{bmatrix} \begin{bmatrix} p_2 \\ q_5 \end{bmatrix} + \begin{bmatrix} 1 \\ 0 \end{bmatrix} [F(t)] \tag{3.8}$$

Case-II: In the plastic deformation or slip phase, the dry friction element velocity V_2 is no longer zero. When spring force builds up and exceeds D, the dry friction force F_f can not counteract F_{spring}, hence the dry friction element slips. In this phase, $F_f = F_{slip} = D$ and the state equations become

$$\begin{bmatrix} \dot{p}_2 \\ \dot{p}_7 \\ \dot{q}_5 \end{bmatrix} = \begin{bmatrix} -\frac{b}{m} & 0 & -k \\ 0 & 0 & k \\ \frac{1}{m} & 0 & -\frac{1}{M_r} \end{bmatrix} \begin{bmatrix} p_2 \\ p_7 \\ q_5 \end{bmatrix} + \begin{bmatrix} 1 \\ 0 \\ 0 \end{bmatrix} [F(t)] + \begin{bmatrix} 0 \\ -1 \\ 0 \end{bmatrix} [D] \tag{3.9}$$

In the complete bond graph of Figure 4.1, the third-order system equations (3.9) are numerically solved, with state variable p_7 being set to zero as necessary when transitioning to the dry element stick phase described by Eq. (3.8).

3.5 Estimation of Physical Parameters

An approximate value of all physical parameters like threshold force (D) of dry friction element, stiffness (k) and damping coefficient (b) can be estimated for a particular bit-rock type using rock mechanical properties and bit geometry. The threshold force of rock is defined as,

$$D = C \cdot A_e \tag{3.10}$$

where C is the compressive strength of rock (Pa) and A_e is the effective contact area (m^2) of the drill bit. According to elastic half-space theory, stiffness and damping coefficient can be estimated using Hsieh's equations as,

$$k = Gr\frac{f_1}{f_1^2 + f_2^2} \tag{3.11}$$

$$b = \frac{r^2}{a_o}\sqrt{G\rho}\frac{f_2}{f_1^2 + f_2^2} \tag{3.12}$$

where a_o is dimensionless frequency, f_1 and f_2 are the Reissner's displacement functions, and a detail description and their value can be found in reference [32]. G is the shear

modulus (Pa), ρ is the density of rock (kg/m^3) and r is the radius of effective contact area (m).

3.6 Specific Energy Equation Formulation

In drilling, energy or power consumption is a major concern. Specific Energy is one of the popular and widely used methods for measurements of drilling efficiency of a particular drilling system [28]. Specific Energy (SE) is defined as the amount of energy (E_h) needed to remove a unit volume (V) of rock, i.e.

$$SE = \frac{E_h}{V} \tag{3.13}$$

Volume of rock removed is defined by

$$V = A_e x$$

where A_e is the area of drill hole (m^2) and x is the penetration depth (m).

Power delivered by the percussion hammer is

$$P_h = \frac{E_h}{\Delta t}$$

where Δt is the time duration (sec) of hammer energy supply.

and rate of penetration

$$R = \frac{x}{\Delta t}.$$

Therefore Eq. (3.13) becomes

$$SE = \frac{P_h}{A_e R} \tag{3.14}$$

A percussive flat button bit is considered for specific energy analysis in this paper. The same bit is assumed for the Performance Index analysis in the next section. The Specific Energy Eq. (3.14) is modified to give "Specific Energy Index (*SEI*)", defined as:

$$SEI = (SE)A_e = \frac{P_h}{R} \tag{3.15}$$

3.7 Formulation of Performance Index

The Specific Energy Index method described in Section 3.3 only reflects the effect of power required to the percussion tool and rate of penetration. Bit wear is another important performance parameter especially for deep percussion drilling where bit changes must be minimized. Additionally, a Performance Index is required that has the freedom to give higher importance to ROP over average hammer power or vise versa through manipulation of weighting factors. Previous methods have not considered bit wear and hence to reflect the effect of bit wear in overall drilling performance, a Performance Index (*PI*) will now be defined as a weighted sum of terms related to rate of penetration, average hammer power (P_{avg}), average force at bit (B_{avg}) and peak force at bit (B_{pk}). It is assumed that bit wear is correlated with bit force and this will be investigated in more detail in future work. The Performance Index is defined as

$$PI = -w_1 \frac{R}{R_{norm}} + w_2 \frac{P_{avg}}{P_{norm}} + w_3 \frac{B_{avg}}{B_{avg_{norm}}} + w_4 \frac{B_{pk}}{B_{pk_{norm}}}$$

where w_1, w_2, w_3 and w_4 are weighting factors selected by the user. Subscript "norm" in above equation indicates values by which individual terms are normalized so that the terms in the equation are non-dimensional. The equation indicates that increased rate of penetration has negative effect whereas others have positive effects on Performance Index during its minimization.

In this investigation, each individual term are normalized with their respective maximum value found in the selected design range, and weighting factors (w_3, w_4) related to bit wear are set to zero as these parameters are in an early stage of investigation.

CHAPTER 4

SIMULATION AND ANALYSIS

4.1 Introduction

In this chapter, model performance is analyzed under different conditions, using the bond graph shown in Figure 4.1, in which the drill bit is subjected to a constant thrust force (weight on bit, WOB) and percussive impact force. In this figure blocks BFavg and BFpk are used to obtain average and peak force respectively at the bit, and send these signals to the Optimization Function block to evaluate SEI and PI.

Table 4.1 lists the mechanical properties of three common rock types from which physical parameters were estimated as shown in Table 4.2. A detail description with a sample example of how the physical parameters are estimated can be found in Appendix B.

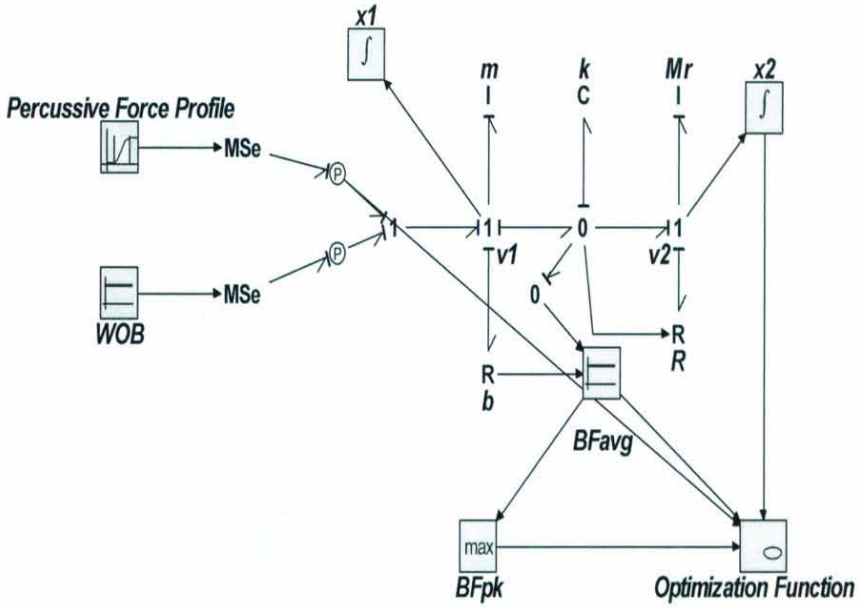

Figure 4.1 Bond graph diagram of rock medium under impact loading

Table 4.1 Mechanical properties of rocks for simulation analysis [31, 33]

Rock Type	*C*, MPa	*E*, GPa	*v*	ρ, kg/m^3
Hackensack Siltstone	123	26	0.22	2590
Berea Sandstone	66.6	15.2	0.37	2100
Pierre Shale I	11	0.9	0.38	2380

Table 4.2 Physical parameters of rocks and bit geometry for simulation analysis

Rock Type & Bit Geometry	*D*, kN	*k*, N/m	*b*, N.s/m
Hackensack Siltstone	380	$2.23\text{x}10^9$	$2.3\text{x}10^5$
Berea Sandstone	206	$1.16\text{x}10^9$	$1.5\text{x}10^5$
Pierre Shale I	34	$6.93\text{x}10^7$	$3.89\text{x}10^4$
Drill bit mass (*m*)	20 kg		
Effective bit radius (r)	0.031418 m		

4.2 System Response to Simple Percussive Loading

To illustrate the typical response of the rock model, a simple percussive type force (Figure 4.2) is applied along with a constant threshold force (206kN) into Berea Sandstone rock medium.

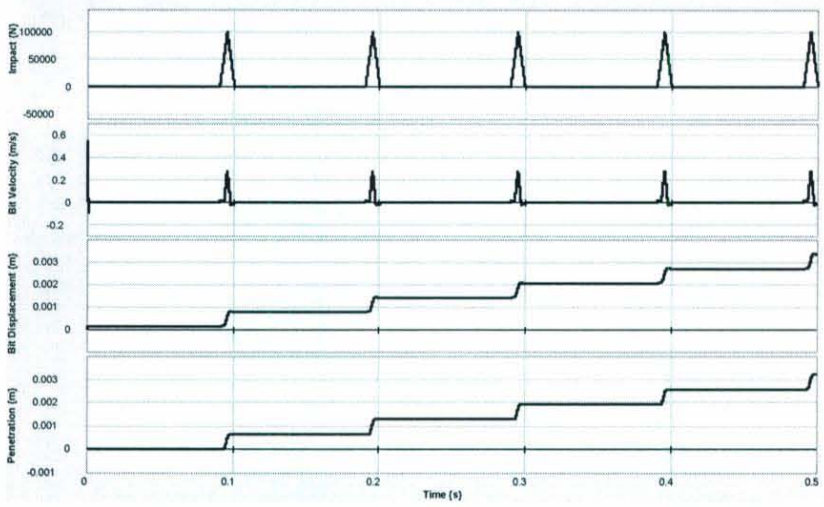

Figure 4.2 Response of rock to simple percussion loading

The top curve ("Impact curve") in Figure 4.2 indicates an impulsive type percussive force profile having short duration (0.01s) and high amplitude (100kN). The bottom curve is the resultant penetration due to the movement of the dry friction element. Each jump in the "Penetration" curve represents failure of rock. The second and third curves show bit velocity and bit advancement due to the applied force.

4.3 Performance of Percussive Loading in Different Rock Formations

To observe the performance of percussive drilling in three different rock formations, an impact force having amplitude 70% of the threshold force along with a constant thrust (WOB) equal to the threshold force of the dry friction element was applied. The impact rise time (T_r) and impact fall time (T_f) are set 0.00025 sec which in combined gives total impact duration.

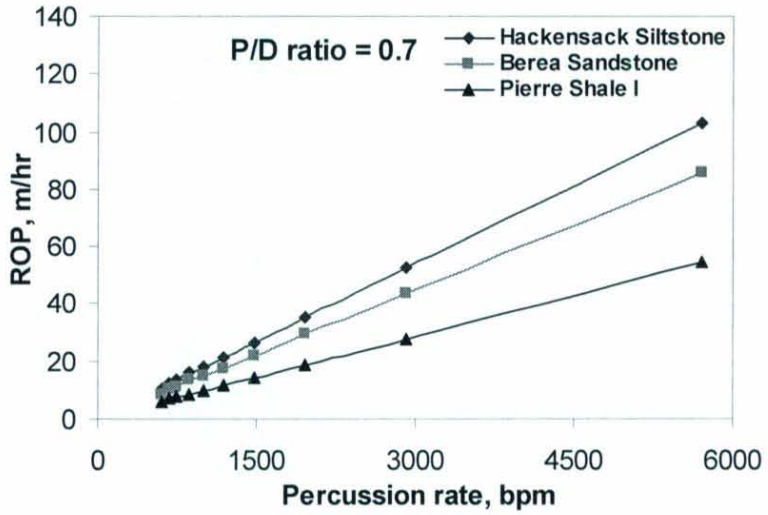

Figure 4.3 *ROP* vs percussion rate for different rock formation (T_r = 0.00025 sec., T_f = 0.00025 sec)

In Figure 4.3, *ROP* in three different rock formations with respect to percussion rate, which is defined in the next section, are plotted by keeping constant impact duration (0.0005sec) but changing the value of gap between consecutive impact blows. From these results, it is observed i) that *ROP* increases with the percussion rate and ii) *ROP* increases with higher rock stiffness at constant *P/D*. Both of these observations are consistent with

theoretical models and experimental data from pioneering percussive drilling research [1, 34]. Having verified that the model behaves as expected, the effect of various force profile parameters on the model outputs that affect Specific Energy Index and Performance Index are studied next.

4.4 Parameter Optimization

The "Time Domain Toolbox" of 20sim was used to analyze performance of percussive force profiles and search for optima. The percussive force profile was defined by the four design parameters as shown in Figure 4.4.

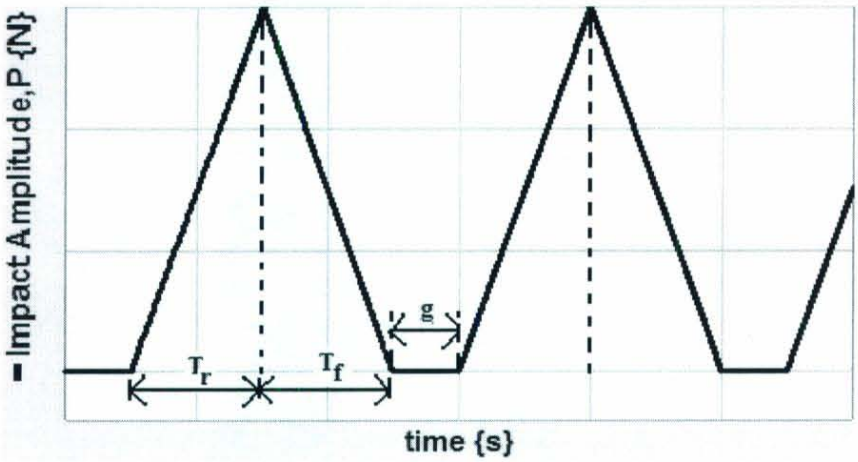

Figure 4.4 Typical percussion force profile defined by P, T_r, T_f, g

The chosen four design parameters are listed in Table 4.3 along with the range over which they were varied. The ranges of parameters were selected in such a way that they closely matched with force profiles generated by real field hammers [4- 7, 13- 14, 23]. Percussion interval is defined as the total sum of impact rise time, fall time and gap between two blows whereas inverse of percussion interval gives percussion rate of the hammer

force profile. In this particular analysis, applied thrust (*WOB*) was kept constant at a level equal to the dry friction threshold force (*D*). Berea sandstone was used as the brittle type rock as mentioned earlier for analysis.

Table 4.3 Design parameters for optimization

Design Parameters	Optimization Range
Impact Amplitude (*P*)	50-150 kN
Gap Between Blows (g)	0.001-0.1 sec
Impact Rise Time (T_r)	0.0001-0.001 sec
Impact Fall Time (T_f)	0.0001-0.001 sec

Initial analysis shows that *ROP* increases when decreasing the percussion interval (increasing the percussion rate while keeping P, T_r, T_f constant but decreasing gap between impact blows) as shown in Figure 4.5. At very low percussion interval (very high percussion rate), an extremely high *ROP* is achieved which is the most important outcome from a drilling system. However, at design points of high percussion rate, the average power required from the hammer is also high and in practical applications such a hammer is not realistic. In this investigation, any design point that gives an unrealistically high rate of penetration and shows extreme power requirements is omitted. Change of average hammer power with *ROP* is shown in Figure 4.6.

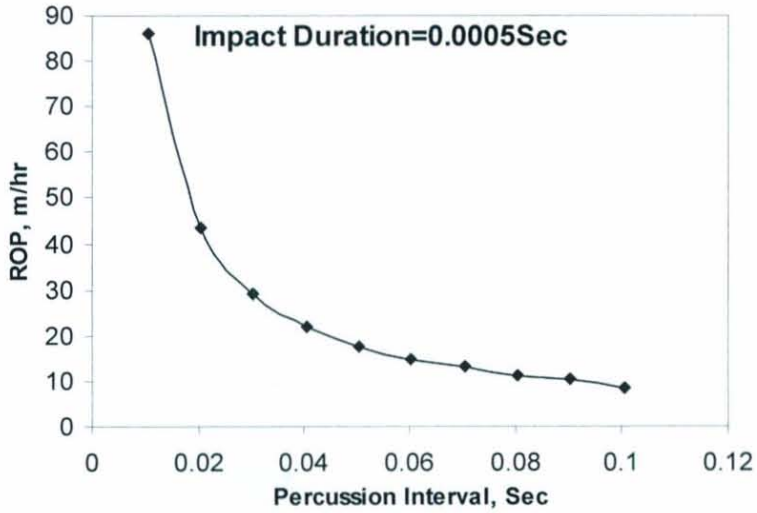

Figure 4.5 Change of *ROP* with percussion interval (P = 150 kN, T_r = 0.00025 sec., T_f = 0.00025 sec.)

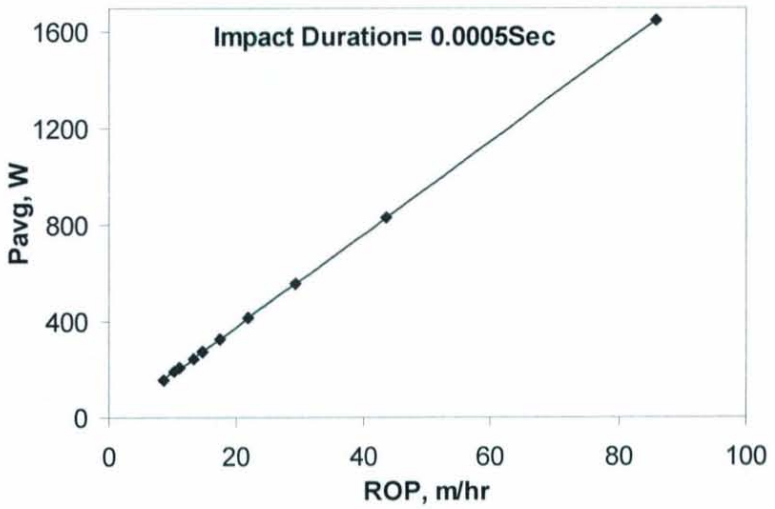

Figure 4.6 Variation of average hammer power with *ROP*. (P= 150 kN, T_r=0.00025 sec., T_f= 0.00025 sec.)

4.4.1 Minimization of Specific Energy

To investigate tradeoffs between this increasing rate of penetration and average hammer power, SEI method as described in Section 3.3 is employed. *SEI* is plotted against percussion rate for single impact duration of 0.0005 sec as shown in Figure 4.7, where impact duration is the sum of impact rise time and impact fall time. It can be seen from Figure 4.7 that symmetric hammer profiles require higher energy than asymmetric profiles and Figure 4.8 indicates that hammers with high impact amplitude required high specific energy.

In summary, among the four design parameters, impact amplitude and gap have higher effect on performance for the short impact durations typical of practical percussion hammers.

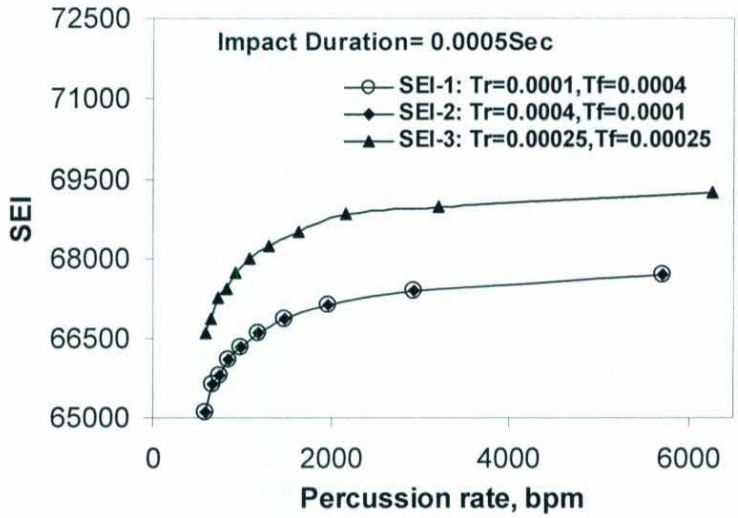

Figure 4.7 Specific Energy Index with percussion rate for impact duration of 0.0005 sec. (P = 150 kN)

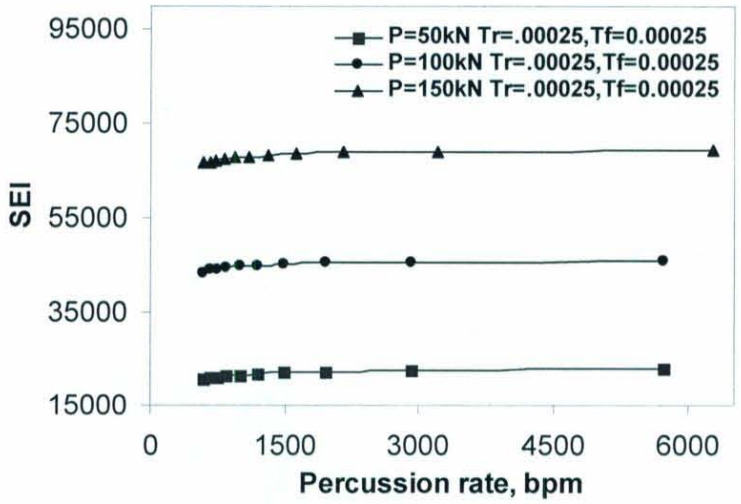

Figure 4.8 Specific Energy Index with percussion rate for different impact amplitude

To minimize SEI over parameter space, an optimization was done using 20sim. The minimum SEI and optimum point from 2401 design points are listed in Table 4.4.

Table 4.4 Optimum design conditions for SEI

P (kN)	T_r (sec)	T_f (sec)	g (sec)	SEI_{min}	P_{avg} (W)	R (m/hr)
50	$1.0e^{-4}$	$1.0e^{-4}$	0.1	10.27	4.08	1.434

Table 4.4 indicates that optimum design point corresponding to minimum *SEI* recommends lowest *ROP* and lowest average hammer power.

4.4.2 Minimization of Performance Index

Now, the PI described in Section 3.4 will be used to generate optima for comparison with those from the *SEI*. To balance the *PI* equation, each performance parameter was

normalized with its individual maximum value found within the design range. Selection of appropriate weighting factor is important for investigating optimum profiles using such *PI*. A Pareto curve is generated for different optimum *PI* values by varying weighting factors w_1 and w_2 are shown in Figure 4.9. At this point, weighting factors (w_3 and w_4) related to bit wear are set to zero.

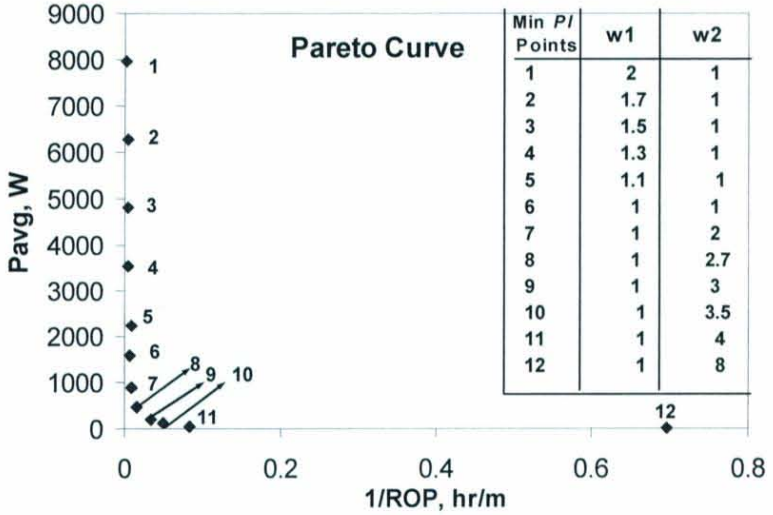

Figure 4.9 Pareto curve showing change in average hammer power with (1/*ROP*) for different optimum *PI*.

From this curve one has the choice to select a hammer profile that will generate higher *ROP* with low hammer power consumption or one can give more concern to power consumption over *ROP*. Table 4.5 lists the minimum *PI* and optimum design points for a particular set of weighting factors (w_1 and w_2).

Table 4.5 Optimum design conditions for different *PI*

Point from Figure 4.9	P (kN)	T_r (sec)	T_f (sec)	g (sec)	P_{avg} (kW)	*ROP* (m/hr)
1	150	$1.0e^{-3}$	$1.0e^{-3}$	0.01	7.94	299.12
2	133.33	$1.0e^{-3}$	$1.0e^{-3}$	0.01	6.27	265.92
3	116.67	$1.0e^{-3}$	$1.0e^{-3}$	0.01	4.8	232.7
4	100	$1.0e^{-3}$	$1.0e^{-3}$	0.01	3.53	199.521
5	116.67	$4.0e^{-4}$	$5.5e^{-4}$	0.01	2.24	121.36
6	66.66	$1.0e^{-3}$	$1.0e^{-3}$	0.01	1.57	133.122
7	50	$1.0e^{-3}$	$1.0e^{-3}$	0.01	0.883	99.92
8	50	$1.0e^{-4}$	$1.0e^{-3}$	0.01	0.47	59.7
9	50	$4.0e^{-4}$	$1.0e^{-4}$	0.01	0.18	28.83
10	50	$1.0e^{-4}$	$2.5e^{-4}$	0.01	0.107	20.5
11	50	$1.0e^{-4}$	$1.0e^{-4}$	0.01	0.045	12.1
12	50	$1.0e^{-4}$	$1.0e^{-4}$	0.1	0.004	1.44

Table 4.5 shows a range of *ROP* and average power at different optimum *PI* points for different sets of weighting factors. It is noticeable that optimum *PI* point 12 (w_1=8, w_2=8) gives the same ROP and average power as obtained from the *SEI* optimum. With the exception of point 12, use of *PI* gives optima with higher *ROP* than obtained from the *SEI* method.

Analysis of both methods indicates that for this visco-elasto-plastic rock model, *SEI* is not a suitable metric because it recommends low percussion rate and low *ROP*. The *PI* strikes a better compromise between *ROP* and power, and *PI* is more useful as it gives freedom to the users to assign weighting factors to penalize power consumption as they see fit. *PI* also has the additional potential benefit of accounting for bit wear.

CHAPTER 5

MODEL VALIDATION AND VERIFICATION

5.1 Introduction

It is important to verify any simulation model with the experimental data in order to ensure its accuracy. In order to validate the visco-elasto-plastic rock model, force-time series, penetration-time series, drill bit geometry, and rock mechanical properties such as compressive strength, density, modulus of elasticity and Poisson's ratio are required. Many researchers conducted experimental investigation and provided F-P information as discussed in Section 2.5. However, not all the experimental results are useful to validate the present rock model as some of the required parameters are not available. Recent experimental work performed by TerraTek (using single cutter impact tester) [22, 43-45], and an experimental investigation done by DRI [48], reflects two different impact

scenarios. However, some simplification and assumption are required to use these tests results for this analysis. In most of the cases, final penetration value is the only criteria to compare model results in the absence of penetration-time series data. More than one reference source is used to get all four mechanical properties for a particular rock type. This selection criterion is justified assuming either the references describing the same rock type or the slight variation in particular rock properties will not significantly effect objective results.

This chapter discusses experimental system layout, instrumentation and measurement criteria followed by the validation procedure.

5.2 Determination of Physical Parameters

All the physical parameters can be estimated from common rock mechanical properties using Eq. (3.10), Eq. (3.11) and Eq. (3.12), as explained in Section 3.2. However, some of the calculated parameters need to be tuned numerically to match the model results. Therefore, new correction factors are introduced to the Eq. (3.11) and Eq. (3.12) for the analysis. Hence, the modified equations of rock stiffness and damping equations can be written as,

$$k = K_s Gr \frac{f_1}{f_1^{\,2} + f_2^{\,2}} \tag{5.1}$$

$$b = K_b \frac{r^2}{a_o} \sqrt{G\rho} \frac{f_2}{f_1^2 + f_2^2} \tag{5.2}$$

Where factor K_s is named as Stiffness Correction factor and K_b as Damping Correction Factor.

Four mechanical properties of different rocks are listed in Table 5.1, and estimated physical parameters using these rock properties along with other simulation parameters are shown in Table 5.2 and Table 5.3. A sample calculation of simulation parameters are shown in Appendix B. Physical parameters listed in Table 5.2 and Table 5.3 are estimated keeping two correction factors K_s and K_b to unity. Description of the experimental setup and bit geometry information used in this analysis are discussed in Section 5.3 and Section 5.4.

Table 5.1 Mechanical properties of different rocks for model validation

Rock Type	*C, MPa*	*E, GPa*	*v*	ρ, kg/m^3
Berea sandstone [43]	45.9	11	0.29	2110
Mancos shale [22, 43,46,47]	55.2	14.47	0.36	2550
Crab Orchard sandstone [22, 46, 47]	138	38.5	0.2	2470
Carthage marble [22, 43,46,47]	115	46.89	0.32	2650
Indiana limestone [51]	62	26	.29	2360

Table 5.2 Estimated physical parameters and bit geometry used to verify TerraTek single cutter impact test results

Rock Type & Bit Geometry	*D, kN*	*k, N/m*	*b, N.s/m*
Berea sandstone	1.453	9.024×10^7	1.34×10^3
Mancos shale	1.764	1.12×10^8	1.65×10^3
Crab Orchard sandstone	4.15	3.4×10^8	2.8×10^3
Carthage marble	3.42	3.7×10^8	3.1×10^3
Drill bit mass (*m*)	1.89 kg		
Bit tip diameter	0.00635 m (0.25in)		
Bit length	0.4648m		

Table 5.3 Estimated physical parameters of Indiana limestone and bit geometry used to verify DRI simple drop test results.

Rock Type & Bit Geometry	*D, kN*	*k, N.m*	*b, N.s/m*
Indiana limestone	900	1.44×10^8	1.00×10^3
Chisel bit mass (*m*)	6.8 kg		
Chisel flat end: (l x w)	(0.75 x 0.03 in)		

5.3 TerraTek Single Cutter Impact test

TerraTek single cutter impact test was employed by Green et al. [22] to investigate deep well hammer drilling performance, and further Han et al. [43-45] refers to the same experimental setup for their analysis. Berea sandstone, Mancos shale, Carthage marble and Crab Orchard sandstone are considered to verify single cutter impact test data and to study the effect of increasing BHP.

5.3.1 Experimental System Layout

A schematic of the TerraTek single cutter impact tester is shown in Figure 5.1. The single cutter having a tip diameter of 0.25 in is attached at the bottom of 18.3 in long steel rod of 1 in diameter, which extends out of the pressure vessel to hold the rock specimen and further extend to the hollow piston. The rock sample is placed inside the pressure vessel. When the gas driven piston strikes the shoulder of the anvil at about its mid length, it generates impact stress wave. This generated stress wave from the shoulder of anvil travels through anvil rod and bit, and reaches to the rock-bit interface. This incoming stress wave is mostly absorbed by the rock and used to produce penetration of bit to the rock. Part of the energy is reflected back as mentioned earlier.

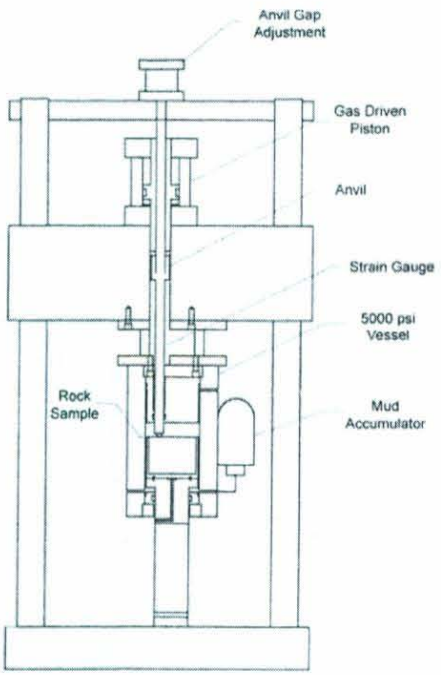

Figure 5.1 Schematic of TerraTek single cutter impact tester [22]

During the test, strain gauges are positioned outside the pressure vessel and on the anvil rod in order to measure impact stress in the anvil. This is considered as the source of input force profile for validation of the present rock model. Another strain gauge is installed at the bottom of the rock surface to observe stress in the rock specimen. A high-frequency resolution laser displacement device is placed on the upper end of anvil to measure displacement of the bit. Data is recorded at about 100k Hz for about one second. The final penetration was measured after the test was completed.

5.3.2 Impact Force Profiles

The physical mechanism for impact force generation was not simulated in the present work, as *20sim* software [30] has the facilities to generate similar force profiles which are close to the real hammer force profiles or experimental force profiles. Further, these force profiles are applied as input force source in to the simulated rock model.

Figures 5.2-5.4 are the regenerated impact force profiles; and those are identical to experimentally obtained force profiles given by Green et al. [22] and Han et al. [43-45]. Figure 5.2 is the force profile of first impact stress wave for duration of 0.6 msec, which is a part of complete test stress profile and recorded before the test is completed. The stress or force profile is recorded for one second to complete the test. The force profile for a complete test as shown in Figure 5.3 is for 0.01 sec as the force magnitudes became zero, and penetration profile also levels off during this time.

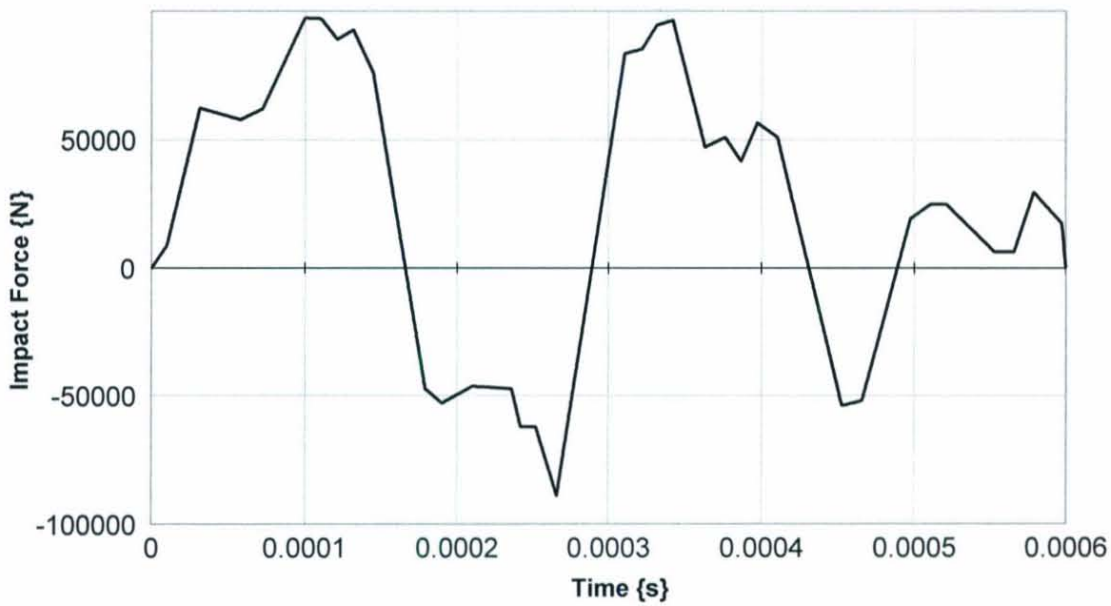

Figure 5.2 Force profile of first impact stress wave for duration of 0.6msec [22, 43-45]

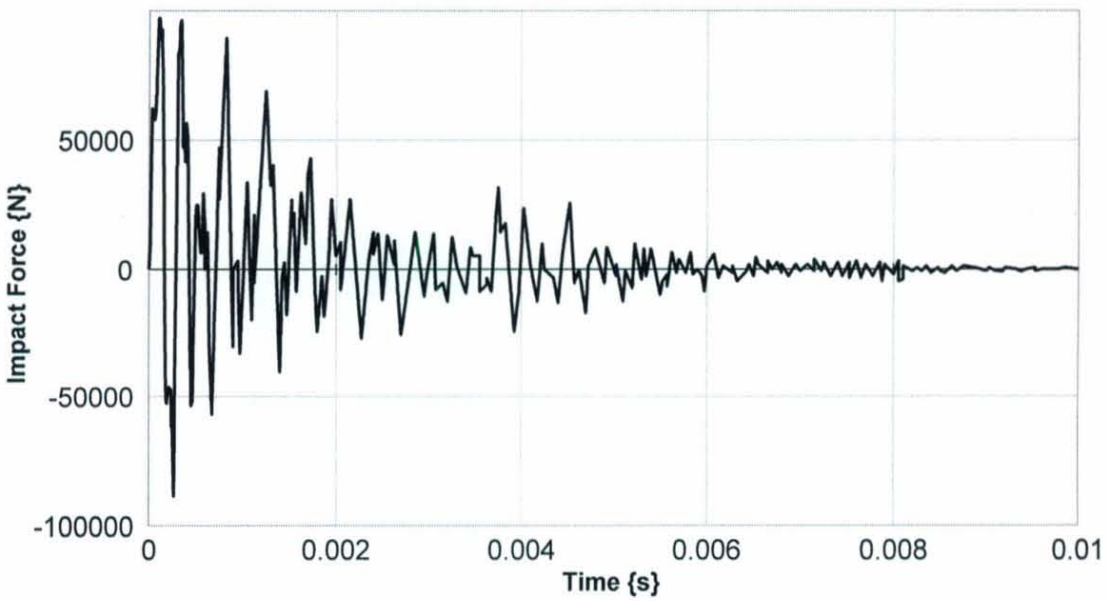

Figure 5.3 Impact force profiles for a complete test [22, 43-45]

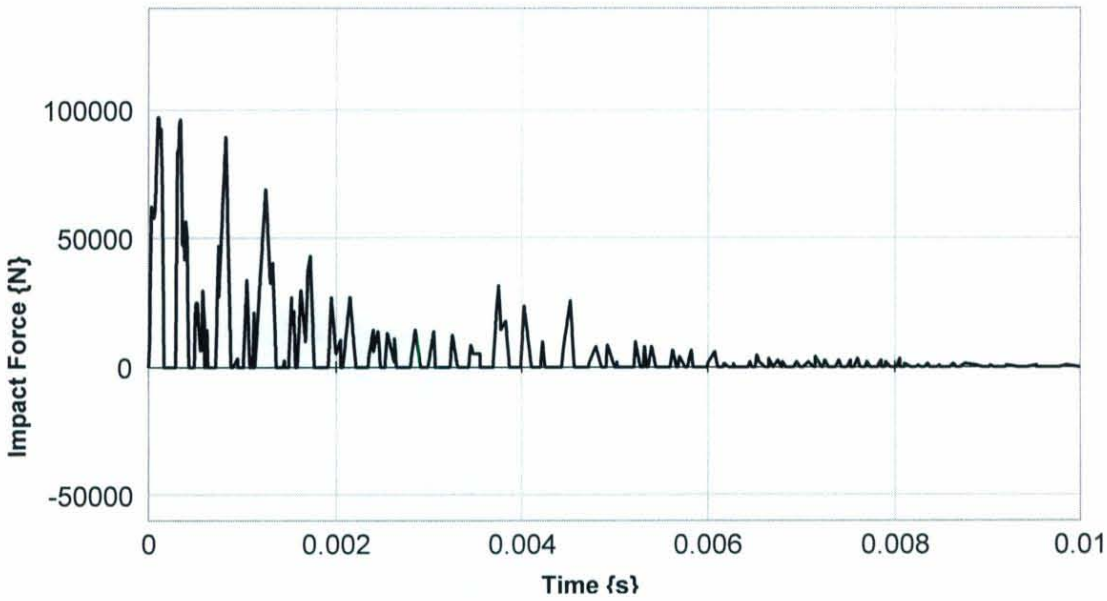

Figure 5.4 Generalized impact force profiles for a complete test neglecting tensile part.

As mentioned earlier, strain gauge for impact load measurement was mounted on a steel anvil rod, therefore compressive part in the measured force profile means during this time the stress wave travels towards the bit-rock interface and during the tensile part the wave travels in the opposite direction. In other words, only the compressive part is responsible for penetration, and tensile force causes no penetration to the rock. Therefore, the impact force profile shown in Figure 5.3 is modified to obtain a more generalized impact force profile setting tensile parts to zero as indicated by Figure 5.4, which is the more appropriate scenario for the present investigation.

5.3.3 Verification of Simulated Rock Model

Berea sandstone is considered for validation using the available penetration profile with first impact stress as well as final penetration data from Figure 5.4. Mancos shale,

Carthage marble and Crab Orchard sandstone are used to study the effect of BHP on final penetration and factor K_b which is the indication of energy dissipation from the rock media due to damping.

5.3.3.1 Single Impact Test on Berea Sandstone

Model penetration and experimental penetration profiles with time are shown in Figure 5.5 for Berea sandstone when the rock is subjected to the impact force of first stress wave. It is observed from the figure that model penetration is not exactly matched with the experimental penetration profile. However, both the penetration profiles are close in magnitude, and hence the model results can be considered as satisfactory for the objective of comparative study between different hammer types.

Figure 5.6 is the plotting of impact force-time and penetration-time curves for the complete 0.01sec test before tuning. The penetration profile is leveled off at a final value of approximately 22 mm whereas experimentally obtained penetration depth was about 6mm [43, 45]. Therefore, the model is tuned to reduce this overestimated penetration by adjusting rock correction factors. During this tuning only K_b is changed whereas K_s is set to unity as K_b is more sensitive to penetration than K_s. Increasing K_b for a rock model indicates that more energy is dissipated from that particular rock medium than predicted using the original model parameters.

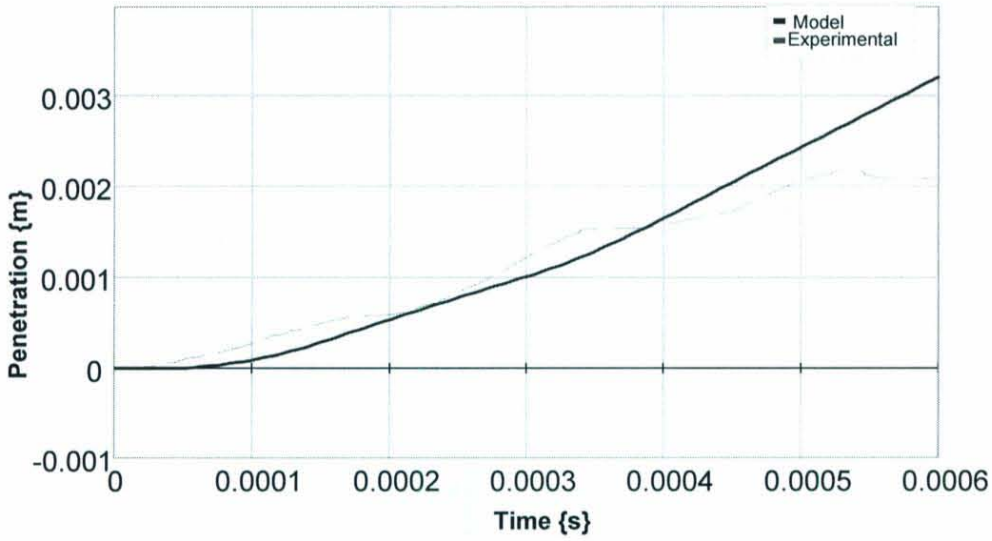

Figure 5.5 Comparison between model and experimental penetration profile due to impact loading of first stress wave (Before tuning i.e. K_s=1, K_b=1).

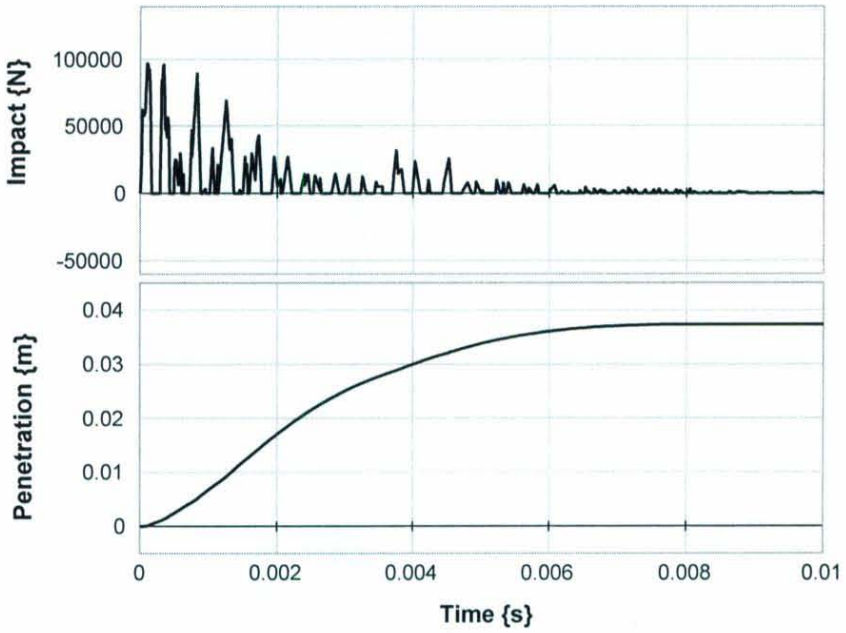

Figure 5.6 Impact force-time and model penetration-time profile for a complete test (Before tuning i.e. K_s=1, K_b=1).

The resultant penetration profile due to impact force from first stress wave and complete test after tuning are shown in Figure 5.7 and 5.8 respectively. A tuning value for K_b equal to 6.4 brings the final penetration to 6mm, although some difference is observed in the case of penetration profile of impact force from first impact stress wave in Figure 5.7.

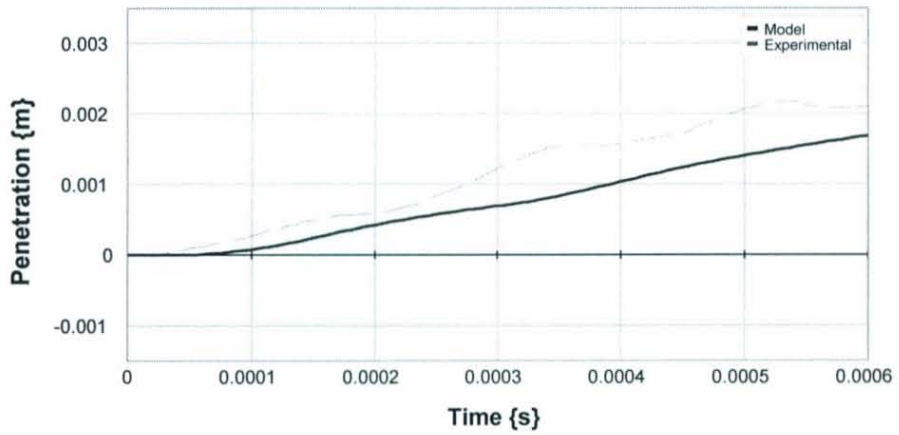

Figure 5.7 Comparison between model and experimental penetration profile due to impact loading of first stress wave (After tuning with K_s=1, K_b=6.4)

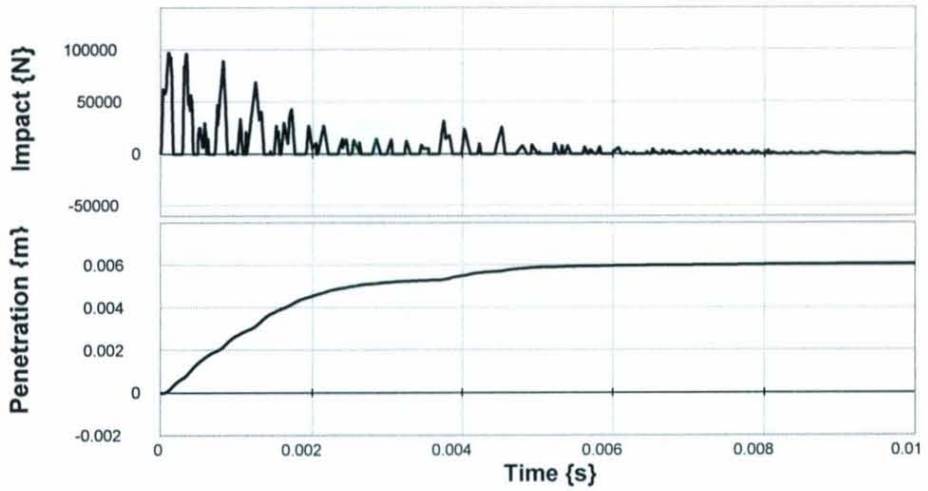

Figure 5.8 Impact force-time and model penetration-time profile for a complete test (After tuning with K_s=1, K_b=6.4).

5.3.3.2 Simulation of Bottomhole Pressure Effect

Mud pressure at the bottomhole of a well is an important phenomenon, which always needs to be considered in the drilling operation as it has a considerable effect on penetration. Therefore, an attempt is made to study the effect of BHP with the help of the present simulated rock model and available experimental test data of Mancos shale, Carthage marble and Crab Orchard sandstone.

Green et al. [22] in their study, mentioned and showed that peak impact load from the first stress wave reduces with the increasing BHP, which subsequently reduces the final penetration. This peak impact load is part of the complete test impact force profile. For this study, it is assumed that the basic shape of force profiles as shown previously in Figures 5.2-5.4 are the same for all BHP conditions but the impact amplitude is different in all cases. The assumption is realistic in a sense that the same impact apparatus is used for all conditions and BHP generates a backward force in opposite direction of applied impact force results a reduction in its amplitude. Therefore, an additional scaling factor, K_f is introduced to scale the magnitude of the generalized force profile shown in Figure 5.4, and to reproduce similar impact force profiles for a particular BHP using,

$$F_{BH}(t) = K_f . F_G(t) \tag{5.3}$$

Where,

$$\text{Force scaling factor, } K_f = \frac{\textit{Peak load at bottomhole mud pressure}}{\textit{Peak load of generalized force profile}}$$

$F_{BH}(t)$ is the impact amplitude for a particular BHP condition at any time t, whereas $F_G(t)$ is the amplitude of the generalized force profile at the same time t. Calculated values of K_f based on available experimental peak load data [22] for different mud pressures are shown in Table 5.4

Table 5.4 Calculated force scaling factor K_f at different borehole mud pressure.

Bottomhole Mud Pressure	0 psi	500 psi	1500 psi	3000 psi
Mancos shale	0.55			0.458
Crab Orchard sandstone	0.57	0.5275	0.481	0.458
Carthage marble	0.6422	0.6422	0.55	0.481

Now, the compressive strength of the rock material will be changed because of the BHP, which can be found by applying different confining pressure through a triaxial test. Compressive strength of the considered rocks is listed in Table 5.4. However, other rock mechanical properties are assumed to be same for the different BHP conditions.

Table 5.5 Compressive strength (MPa) of rocks at different borehole mud pressure conditions.

Bottomhole Mud Pressure	0 psi	500 psi	1500 psi	3000 psi
Mancos shale	55.16			114.9
Crab Orchard sandstone	137.9	168.54	229.83	303.38
Carthage marble	115	122.57	141.37	172.375

In this analysis four different BHP conditions from a range of 0 to 3000 psi are considered for Carthage marble and Crab Orchard sandstone. In case of Mancos shale, it is found that the experimental final penetration at 500 psi BHP is lower than the

penetration at 1500 psi BHP which is abnormal, and hence these two data points were neglected from the analysis. The analyzed model penetration results along with experimental values for these three rocks are shown in Figures 5.9-5.11.

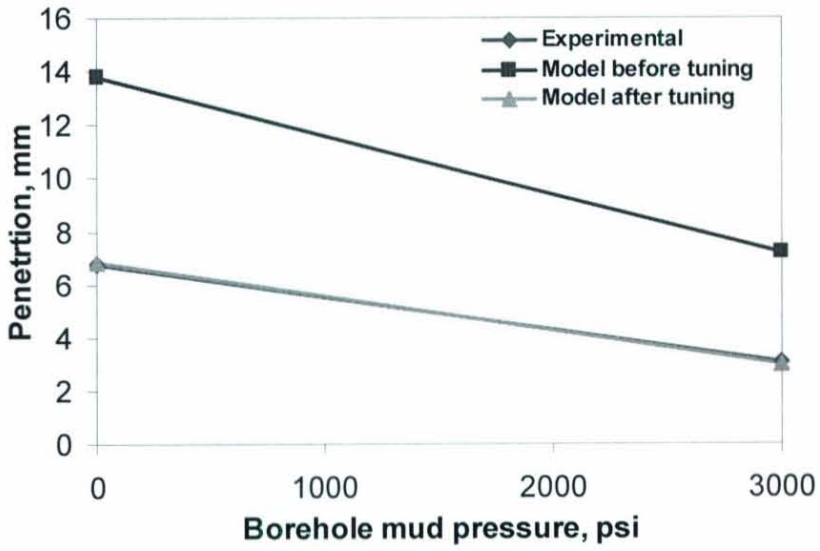

Figure 5.9 Effect of BHP on penetration for Mancos shale

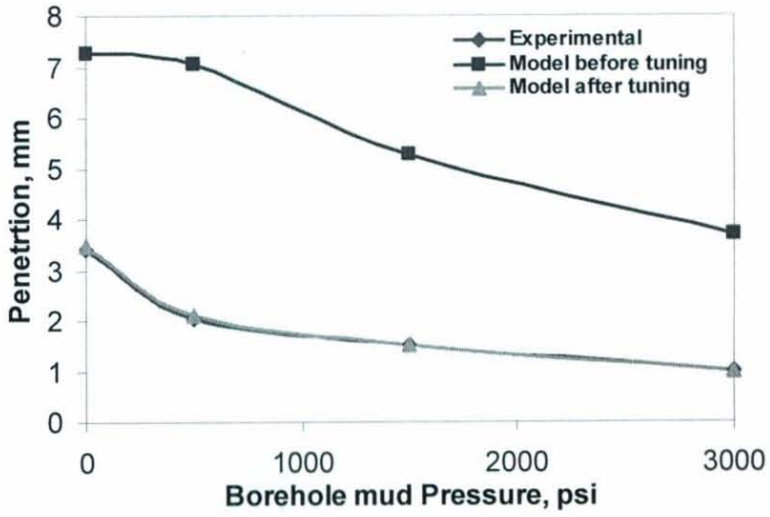

Figure 5.10 Effect of BHP on penetration for Carthage marble

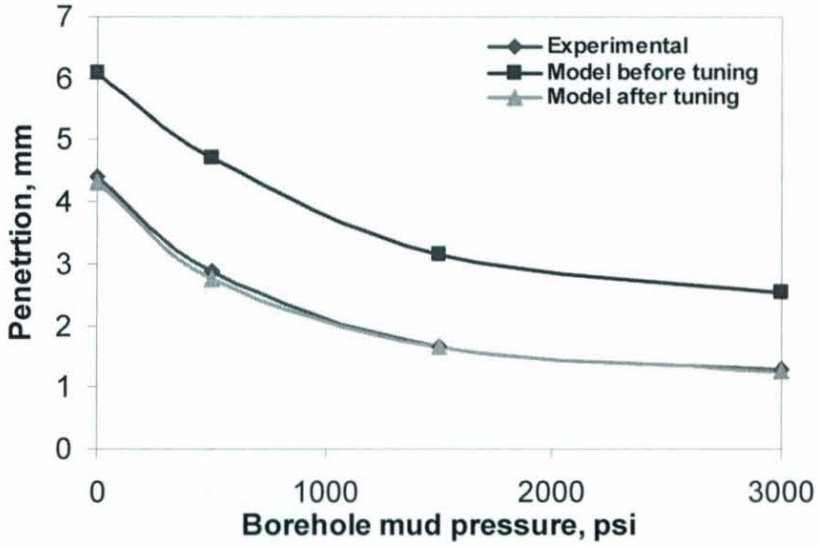

Figure 5.11 Effect of BHP on penetration for Crab Orchard sandstone

Figures 5.9-5.11 contains model penetration before tuning, experimental final penetration provided by Green et al. [22] and model penetration results after tuning. Model force-time and penetration-time (after tuning) plots are shown in Appendix C.

The results indicate that the penetration significantly decreases due to increasing BHP for all rock types, which is consistent with the experimental results. Both the model results before tuning and experimental profiles follow the same pattern, however there is some variation in their magnitude. Therefore, the rock model is tuned to match with experimental results again by changing only the value of K_b. The values of K_b are shown in Figure 5.12 for tuning at different BHP, which indicates that the value of K_b increases linearly with BHP. In practice, a part of the applied hammer energy is absorbed by the bottomhole fluid, and hence it reduces the amplitude of the impact force, which is

responsible for the rock fracture. Therefore, the presence of borehole fluid reduces the rock penetration significantly, and increment in K_b with BHP completely supports the obtained model results.

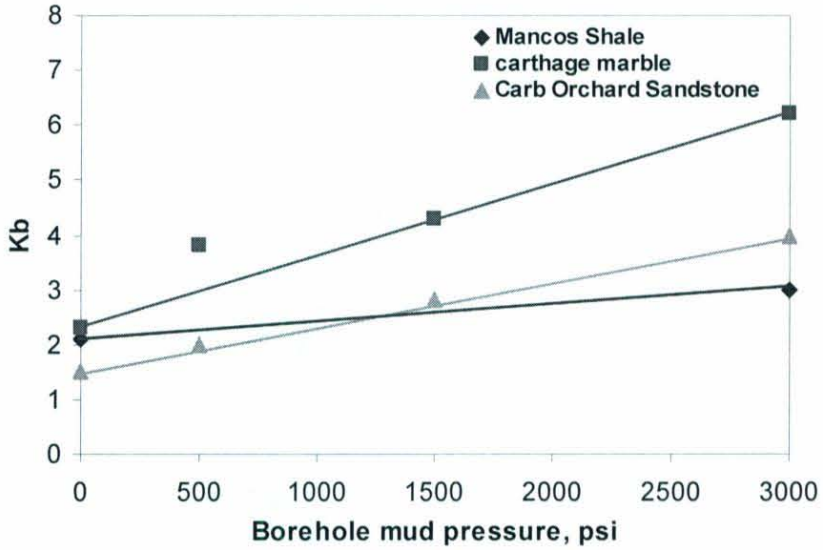

Figure 5.12 Effect of BHP on K_b for different rocks.

5.4 DRI Simple Drop Test

Another approach to study the rock response under simple impact is to use drop tests as done by DRI [48]. Impact force profiles of the DRI drop tester are different from TerraTek Single Cutter force profiles in the sense that there is no tensile part in DRI tested force profiles. This section describes the verification process of rock model with DRI executed drop test on Indiana limestone from four different drop heights.

5.4.1 Experimental System Layout

Experimental setup of the DRI drop tester is shown in Figure 5.13. The apparatus consists of a cylindrical mass block of 15lb which is guided through two guide rods, and it can freely fall on the rock specimen from different drop height or energy level. A chisel type bit having a chisel edge ¾ in long with a 0.03 in wide flat end is attached to the bottom of the mass block.

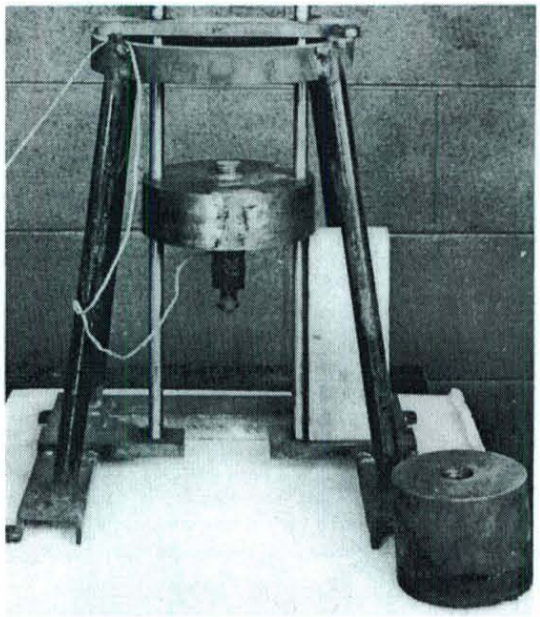

Figure 5.13 Experimental setup of DRI drop tester [48]

Strain gauges are mounted close to the bit to measure impact force at the bit-rock interface. An oscilloscope camera is used to record the force waveform. Displacement-time and velocity-time records are obtained from a high speed motion camera at about 3000Hz.

5.4.2 Impact Force Profiles

Force waveforms measured at the bit from DRI drop test on Indiana limestone for four different drop heights are shown in Figure 5.14.

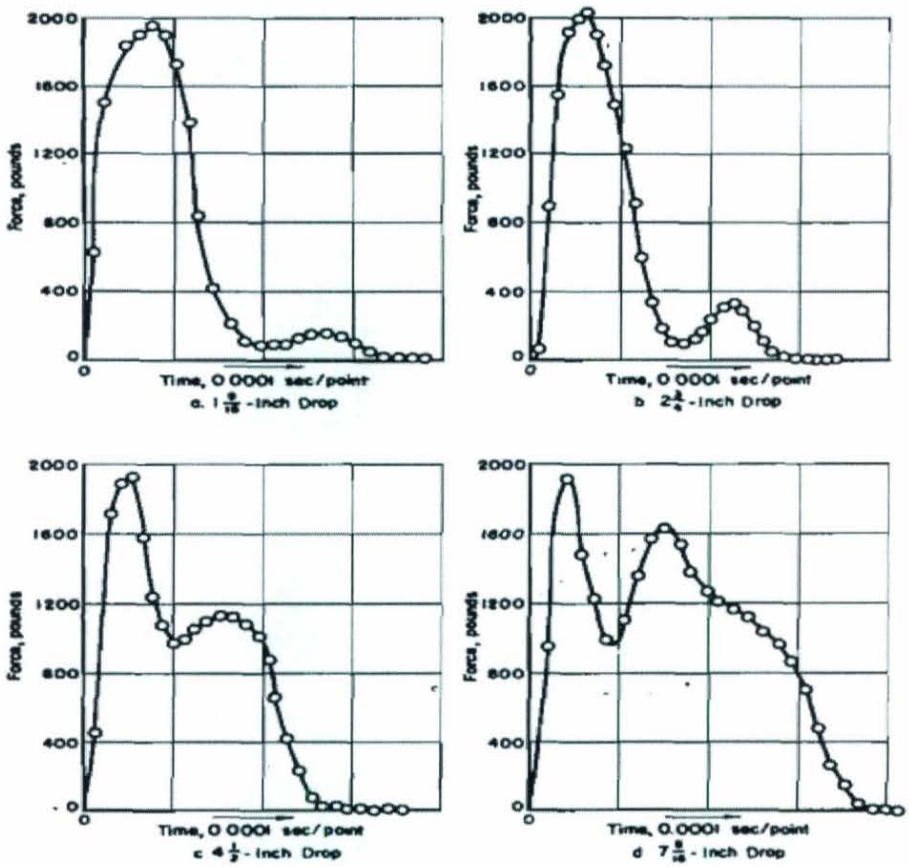

Figure 5.14 Typical impact force profiles for various drop heights [48]

Figure 5.14 indicates that the first peak appears at about 200 lb for all drop heights and the profiles follow a decrement in their amplitude. A second peak is also observed which increases with the drop height. For the height below 9/16 in, the second peak is absent for falling heights between 9/16 in and 6 in the second peak developed, and above 6 in of

drop height it is assumed that the second peak is constant in magnitude. For convenience, units of all quantities are converted into metric units for the entire analysis.

5.4.3 Verification of Simulated Rock Model

The objective of this section is to study the response of the rock model, and to observe how the factor K_b is changed with different impact energy level when subjected to impact forces shown in Figure 5.14. Final penetration value from a force-displacement curve [48] is compared with model penetration in the absence of any displacement-time series. The regenerated bit force-displacement curves for four different heights are presented by Pennington [48] are shown in Figure 5.15. Finally, a comparative study is also done to observe how the slope of a force-displacement curve is changed with drill bit mass.

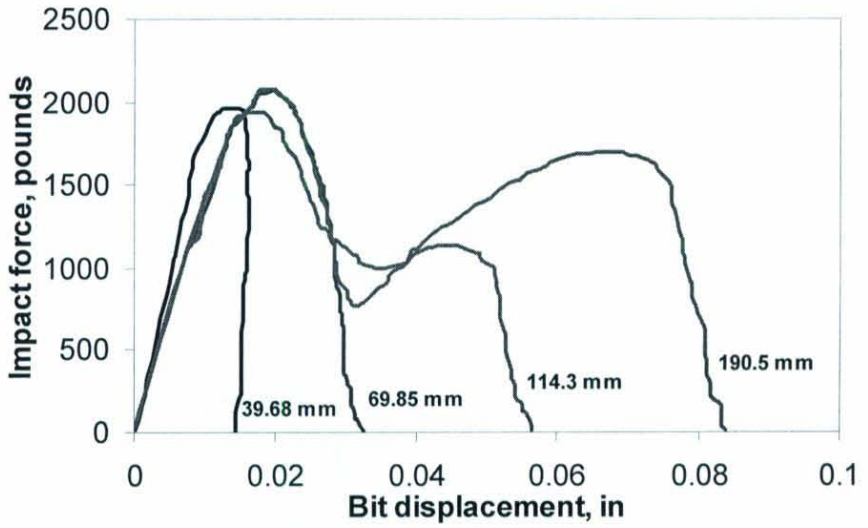

Figure 5.15 Regenerated experimental bit force displacement curves for Indiana limestone from four different drop heights [48].

5.4.3.1 Drop Test on Indiana Limestone

When the energy level of the impact system increases the rock penetration also increases linearly which is indicated by the penetration vs. drop height curves in Figure 5.16. Figure 5.16 contains three different curves, model penetration before tuning, experimental penetration and model penetration after tuning. The results in this figure illustrate that there is no significant difference between the curves except some variation in magnitude which is observed for the model penetration before tuning curve. Therefore, the model is tuned by changing factor K_b to match the experimental results. The values of factor K_b are shown in Figure 5.17, which indicates that K_b decreases with drop height.

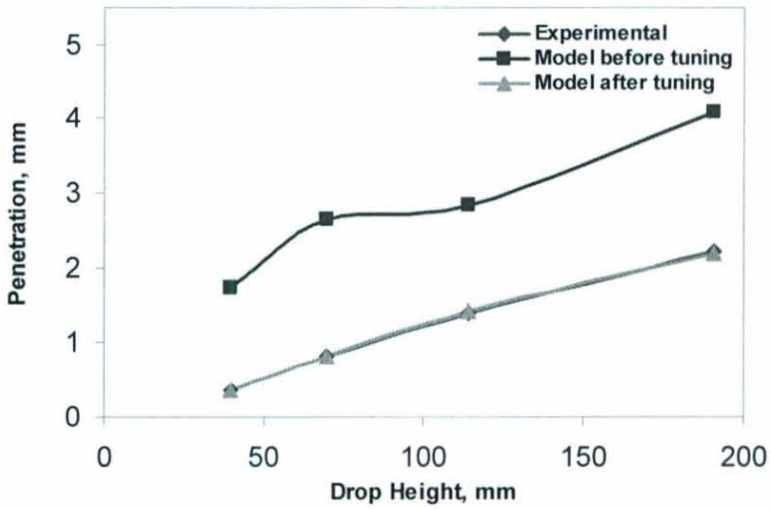

Figure 5.16 Penetration results in Indiana limestone due to different drop height.

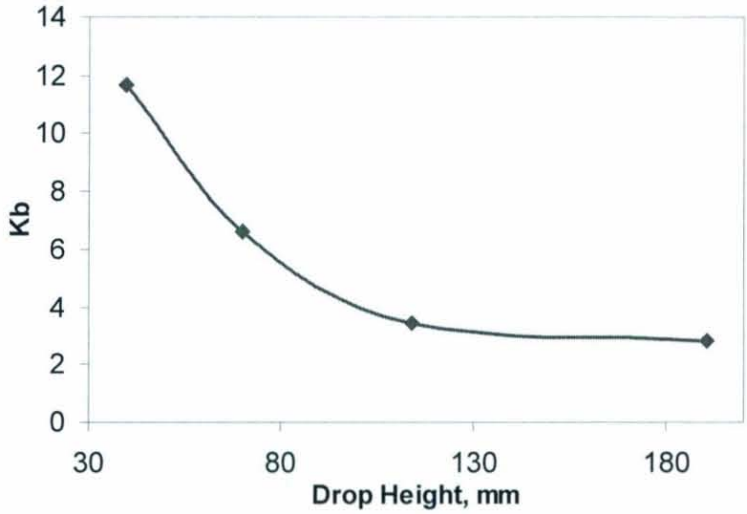

Figure 5.17 Change of K_b for tuning model penetration.

As mentioned earlier, experimental penetration values of Figure 5.16 are taken from force-displace curves which are shown in Figure 5.15. A plot of force vs. bit displacement from the simulated rock model and considering different drill bit masses is shown in Figure 5.18. A significant difference is observed between model bit force-displacement curves and experimental force-displacement curves in their initial slop. The model generates force-displacement curves with very high slop, and when the bit mass decreases the initial slope of the curve also decreases which can be observed more closely in a zoomed view of Figure 5.18 and shown in Figure 5.19. Figure 5.19 indicates that the slop of the curve decreases with decreasing bit mass. These results helped to understand the possible reasons for the differences between model and experimental force-displacement curves. The strain gauges for impact force measurement is installed close to the bit, which means that the impact force is measured directly at the bit-rock interface but in the case of

developed visco-elasto-plastic rock model the impact force is applied on the bit mass, and hence due to the inertia effect of bit mass the model provide bit force-displacement profile with higher slop. However, the model is very much useful and proved its effectiveness in comparative study even without this difference.

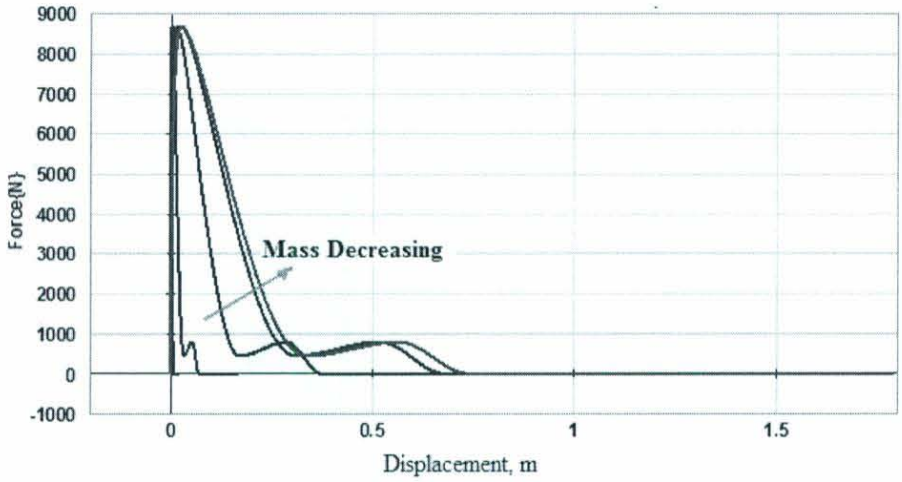

Figure 5.18 Model force-displacement curve for different bit mass (Drop height 39.5mm)

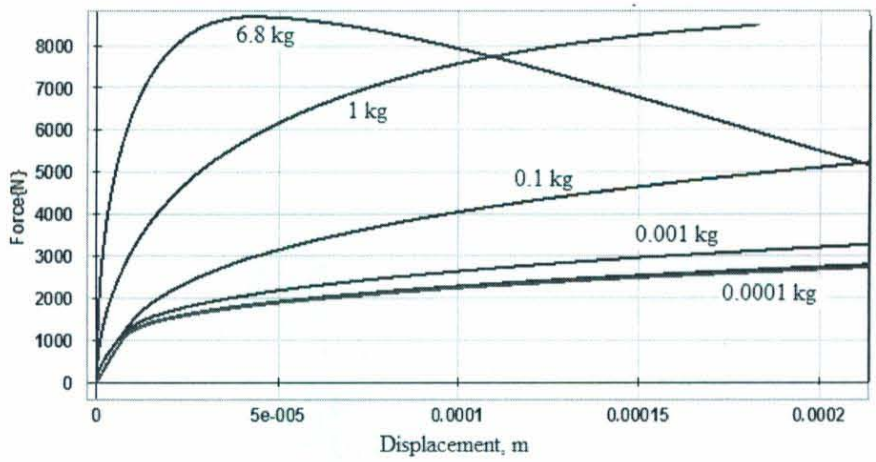

Figure 5.19 Zoomed view of model force-displacement curve for different bit mass (Drop height 39.5mm)

CHAPTER 6

SUMMARY AND CONCLUSIONS

6.1 Summary of Present Work

Previous research work has established that percussion drilling gives higher penetration than conventional rotary drilling. The oil and gas industry is also concerned about the power or energy required to achieve this performance as power requirement also increases with rate of penetration. The main motivation of this present work is to guide the design and development of an optimal percussion tool by investigating the effect of different percussive force profiles on rate of penetration, energy requirements and predictors of bit wear in hard rock drilling.

The present work gives a brief overview of percussive drilling, points out its potential benefits over other technologies, associated negative factors, and most importantly

explains fundamental process involved in rock failure under percussion loading (which is very much essential to characterize percussive drilling).

The modeled rock is assumed to behave visco-elastically before failure and to plastically deform post-failure. A range of hammer force profile shape parameters are selected to generate impact force profiles demonstrating a real field percussion hammer drilling scenario. The model test and analysis of different rock formations under percussion is a good illustration to observe how the penetration changes with rock strength.

In this investigation a methodology is presented to estimate physical parameters of the rock model, which is always a difficult and challenging task faced by different authors and researchers. Here, the model results are satisfactory using these estimated parameters, and little effort is required to tune the model with the experimental results.

This work describes a Specific Energy Index developed by other researchers which suggested optima with low rate of penetration and low power input, as well as a new performance index which has potential advantages over SEI.

The model results are analyzed and verified with the experimental results from TerraTek single cutter impact test and DRI drop test, which illustrates how the BHP and drop height effects the final penetration for different rock formations.

The drilling mud system or fluid flow system is not involved in the developed rock model, however a method is shown to study the effect of BHP on penetration mechanism and energy dissipation due to damping. The results indicate that BHP significantly reduces the penetration and increases the damping energy loss, which is completely in agreement with real field drilling operation. Based on the results, one can easily establish a relationship between BHP and penetration as well as BHP and damping for a given rock material properties and impact force. This is helpful to predict performance in different formations before carry out any drilling operation.

Another interesting observation can be made from the model performance test results described in chapter 4 and model verification results discussed in chapter 5. In the first case, a thrust force or WOB is considered however in the second case it is neglected. It is known that a thrust force is applied to keep bit in contact with rock during field percussion drilling, but in the laboratory environment simple impact system or drop test system doesn't have WOB. Therefore, this work involves validation of the rock model using laboratory experimental results [22, 43-45, 48] as well as some analysis of field drilling conditions.

Although the presented work has been directed towards the design of a percussive hammer tool, the model studied here can be used to investigate other types of impact loading like vibration-assisted drilling.

6.2 Limitation of Present Work

It is challenging to predict penetration rate in rock under vibro-impact force because of rock's complex behavior. Percussion drilling or any other drilling system must have to perform two separate functions to achieve penetration in the rock medium: 1. fracture and failure of rock materials and 2. ejection of rock cuttings. The first phase is basically the actual penetration of the system, while the second is rock cuttings removal. Both phases are important for the drilling and drilling performance. A major limitation of the visco-elasto-plastic model is that it only considered the first phase of the drilling system and neglected the second phase, resulting in an overestimated rate of penetration. Although the absolute predictions of the presented model may not be completely accurate in the absence of field drilling data, the model is a good platform from which to evaluate and compare different percussive force profiles. Some other assumptions and limitations:

- The model does not account for bit rotation or blow indexing which enables the bit to strike the rock in different spot on consecutive blows. This may result in under prediction of ROP for certain parameters.
- The model has linear stiffness and viscous damping.
- The model does not account for the size and shape of the drill bit and drill hole.
- The model does not account for fluid flow which takes significant time to clean the hole, control dust, cool the bit and stabilize the hole.
- Physical mechanism of impact force generation is not simulated. Input impact force profile is directly applied to the model.

- This work mentioned the importance of bit wear in percussion drilling which is also considered in PI function however due to the unavailability of experimental information bit wear investigation is not incorporated in the analysis.
- The model doesn't consider fatigue failure or change of rock medium property due to dynamic loading.
- The model validation process is dependent on a few sources of experimental data.

6.2 Recommendations for Future Work

As an extension of the work, an experimental setup is now under way to calibrate the rock model for different formations and to learn more about actual impact force profiles. The experiment involves single impact drop tests to determine penetration and force profiles for a small button bit. Energy supplied into the system will be controlled by adjusting the height and weight of a free falling mass. The experimental data will be used to tune visco-elasto-plastic rock model parameters in the next phase of this investigation. After validation and calibration, the simulation tool will be used in the design of a vibration or percussion-assisted rotary drilling tool. Based on achievements and limitations of the present investigation the following research scope can be recommended,

- An introduction of blow indexing or rotary drilling action into the developed model will be helpful to study the system in conventional rotary and rotary-percussion drilling mode.

- Simulation of rock cuttings removal process and mud fluid flow system along with the present rock model will be useful to study real field drilling conditions.
- More analysis on the sensitivity of simulation parameters like bit mass, stiffness, damping coefficient are required to better understand the system behavior.
- An extensive investigation on hammer energy requirement, energy transformation efficiency, bit wear, rock fatigue failure under dynamic loading will be beneficial for percussion drilling.

REFERENCES

1. Hustrulid, W. A. and Fairhurst, C. (1970). "A Theoretical and Experimental Study of the Percussive Drilling of Rock, Part-1-Theory of Percussive Drilling". *International Journal of Rock Mechanics & Mining Sciences*. Vol. 8, pp. 311-333.

2. Han, G., Bruno, M and Lao, K. (2005). "Percussion Drilling in Oil Industry: Review and Rock Failure Modelling". *American Association of Drilling Engineers.* AADE-05-NTCE-59.

3. Pixton, D. and Hall. "A New-Generation Mud-Hammer Drilling Tool". Annual Report, Novatek, Inc.

4. Han, G., Bruno, M. and Dusseault, M. B. (2005). "Dynamically Modeling Rock Failure in Percussion Drilling". *American Rock Mechanics Association.* ARMA/USRMS 05-819.

5. Fairhurst, C. (1959). "Energy Transmission in Percussive Drilling". *Society of Petroleum Engineers of AIME*. Paper no 1287-G.

6. Hustrulid, W. A. and Fairhurst, C. (1970). "A Theoretical and Experimental Study of the Percussive Drilling of Rock, Part-II –Force-Penetration and Specific Energy Determination". *International Journal of Rock Mechanics & Mining Sciences.* Vol. 8, pp. 335-356.

7. Hustrulid, W. A. and Fairhurst, C. (1970). "A Theoretical and Experimental Study of the Percussive Drilling of Rock, Part-III-Experimental Verification of the

Mathematical Theory". *International Journal of Rock Mechanics & Mining Sciences.* Vol. 9, pp. 417-429.

8. Simon, R. (1963). "Energy Balance in Rock Drilling". *Society of Petroleum Engineers*. SPE 499.

9. Burdine, N. T. (1963). "Rock Failure Under Dynamic Loading Conditions". *Society of Petroleum Engineers*. SPE 481.

10. Kou, S. Q., Liu, H. Y., Lindqvist, P.A. and Tang, C. A. (2004). "Rock Fragmentation Mechanisms Induced by a Drill Bit". *International Journal of Rock Mechanics & Mining Sciences*. Vol. 41, No.3, CD-ROM.

11. Topanelian, E. J. (1958). "Effect of Low Frequency Percussion in Drilling Hard Rock". *Technical note 2013*. SPE 878-G.

12. Chang, E. L. (2004). "Dynamic Force-Penetration Curves in Rock by Matching Theoretical to Experimental Wave Propagation Response". *Society of Experimental Mechanics.* Vol. 44, No. 2.

13. Chiang, E. L. and Elias, D. A. (2007). "A 3D FEM Methodology for Simulating the Impact in Rock-Drilling Hammers". *International Journal of Rock Mechanics & Mining Sciences* 45(2008)701-711.

14. Izquierdo, E. L. And Ching, L. E. (2004). "A Methodology for the Estimation of the Specific Rock Energy Index Using Corrected Down-The–Hole Drill Monitoring Data". *Mining Technology (Trans. Inst. Min. Metal. A).* Vol. 113.

15. Chiang, L. E. and Elias, D. A. (1999). "Modeling Impact in Down-The-Hole Rock Drilling". *International Journal of Rock Mechanics & Mining Sciences* 37(2000) 599-613.

16. Lundberg, B. and Okrouhlik, M. (2005). "Efficiency of a Percussive Rock Drilling Process with Consideration of Energy Radiation into the Rock". *International Journal of Impact Engineering* 32 (2006) 1573-1583.

17. Pavlovskaia, E. and Wiercigroch, M. (2003). "Modelling of Vibro-Impact system Driven by Beat Frequency". *International Journal of Mechanical Sciences* 45(2003) 623-641.

18. Wiercigroch, M., Krivtsov, A. M. and Wojewoda, J. (2008). "Vibrational Energy Transfer via Modulated Impacts for Percussive Drilling". *Journal of Theoretical and Applied Mechanics* 46, 3, pp. 715-726.

19. Fernando, L., Franca, P. And Weber, H. I. (2003). "Experimental and Numerical Study of a New Resonance Hammer Drilling Model with Drift". Chaos, Solitons and Fractals 21 (2004) 789-801.

20. Batako, A. D., Babitsky, V. I. and Halliwell, N. A. (2003). "Modelling of Vibro-Impact Penetration of Self–Exciting Percussive-Rotary Drill Bit". *Journal of Sound and Vibration* 271(2004) 209-225.

21. Li, Y., Ting, K. L. and Lei, B. (2001). "Simulation on the Vibration of the Hydraulic Hammer". *ASME 2001. Design Engineering technical Conference and Computers and Information in Engineering Conference.* DETC2001/VIB-21774.

22. Green, S., Judzis, A., Curry, D., Black, A., Prasad, U. and Rogers, J. (2005). "Single Cutter Impact Tests Investigate Deep-Well Hammer-Drilling Performance". SPE 97173.

23. Chitty, D. E., Blouin, S.E., Zimmer, V. L., Thompson, P. H. and Tremba, E. L. (2005). "Rotary Percussion Sounding System for In situ Rock Mass Characterization". *American Rock Mechanics Association.* ARMA/USRMS 05-868.

24. Reddish, D.J., Stace, L. R., Vanichkobchinda, P. and Whittles, D.N. (2004). "Numerical Simulation of the Dynamic Impact Breakage Testing of Rock". *International Journal of Rock Mechanics & Mining Sciences* 45(2005)167-176.

25. Wilson, D. C. and Bentsen, R. G. (1972). "Optimization Techniques for Minimizing Drilling Costs". *Society of Petroleum Engineers of AIME.* SPE 3983.

26. Iqbal, F. (2008). "Drilling Optimization Technique- Using Real Time Parameters". SPE 114543.

27. Karnopp, D. C., Margolis, D. L. and Rosenberg, R. C. (2006). "*System Dynamics-Modeling and Simulation of Mechatronic System*". 4th Edition: John Willey & Sons,Inc.

28. Kennedy, B. A. et al. (1990). "Mine Operations". In *Surface Mining*, 2nd Edition. pp. 513-522.

29. Karnopp, D. (1985). "Computer Simulation of Stick-Slip Friction in Mechanical Dynamic Systems". *American Society of Mechanical Engineers.* Vol. 107 pp. 100-103.

30. 20sim version 4.0, Control lab Products b.v, Enchede, Netherlands.

31. New England Research Inc. "Elastic constants and strength of Berea Sandstone". www.ner.com.

32. Richard, F. B. Jr. et al. (1970). "Theories for Vibrations of Foundations on Elastic Media". In *Vibration of Soils and Foundations*. Prentice-Hall, Inc. 194-203

33. Fjaer, R. M. H., Horsrud, P., Raaen, A. M. and Risnes, R. (2008). "Appendix A". In *Petroleum Related Rock Mechanics*, 2nd Edition. Elsevier. 438.

34. Hustrulid, W. A. and Fairhurst, C. (1970). "A Theoretical and Experimental Study of the Percussive Drilling of Rock, Part 1V- Application of the Model to actual Percussive Drilling". *International Journal of Rock Mechanics & Mining Sciences.* Vol. 8, pp. 311-333.

35. Pierce, K. G., Livesay, B. J. and Finger, J. T. (1996). "Advanced Drilling Systems Study". Report. Sandia National Laboratories. SAND95-0331.

36. Butt S. D. (2009). "Advanced Exploration Drilling Technology". Project Overview.

37. Niu, D. (2008). "Rigid Impact- the Mechanism of Percussive Rock Drilling". *American Rock Mechanics Association.* ARMA 08-075.

38. Liu, Y., Bar-Cohen, Y. and Chang, Z. (2007). "Analytical and Experimental Study of Determining the Optimal Number of Wedge Shape Cutting Teeth in Coring Bits Used in Percussive Drilling". *Journal of Manufacturing Science and Engineering.* Vol. 129, pp. 760-769.

39. Appl, F. C. and Gatley, W.S. (1962). "Rate-of-Loading Effects in Chisel Impact". *Society of Petroleum Engineers.* SPE 167.

40. Podio, A. and Gray, K. E. (1965). "Single-Blow Bit-Tooth Impact Tests on Saturated Rocks Under Confining Pressure: I. Zero Pore Pressure". *Society of Petroleum Engineers*. SPE 1056. Vol. 5, pp. 211-224.

41. Yang, J. H. and Gray, K. E. (1967). "Single-Blow Bit-Tooth Impact Tests on Saturated Rocks Under Confining Pressure: II. Elevated Pore Pressure". *Society of Petroleum Engineers*. SPE 1702.

42. Hartman, H. L. (1963). "The Simulation of Percussion Drilling in the Laboratory by Indexed-Blow Studies". *Society of Petroleum Engineers Journal*. SPE 500.

43. Terralog Technologies Inc (USA). (2005). "Fundamental Research on Percussion Drilling: Improved Rock Mechanics Analysis, Advanced Simulation Technology, and Full Scale Laboratory Investigations". Final report. 2nd Version. DE-FC26-03NT41999.

44. Han, G. and Bruno, M. (2006). "Percussion Drilling: From Laboratory Test to Dynamic Modeling". *Society of Petroleum Engineers Journal*. SPE 104178.

45. Han, G. and Bruno, M. (2006). "Lab Investigation of Percussion Drilling: From Single Impact to Full Scale Fluid Hammer". *American Rock Mechanics Association.* ARMA/USRMS 06-962.

46. Walker, B. H. et al. (1986). "Roller-Bit Penetration Rate Response as a Function of Rock Properties and Well Depth". *Society of Petroleum Engineers Journal*. SPE 15620.

47. Black, A. D. et al. (2008). "Optimization of Deep Drilling Performance with Improvements in Drill Bit and Drilling Fluid Design". *IADC/SPE Drilling Conference*. IADC/SPE 112731.

48. Pennington, J. V. (1953). "Some Results of DRI Investigations-Rock Failure in Percussion". Drilling Research, Inc. 33rd Annual Meeting of the Institute, Chicago.

49. Kahraman, S., Bilgin, N. and Feridunoglu, C. (2003). "Dominant Rock Properties affecting the Penetration Rate of Percussive Drills". *International Journal of Rock Mechanics and Mining Sciences 40 (2003) 711-723.*

50. Han, G., Bruno, M. and Dusseault, M. B. (2005). "Dynamically Modelling Rock Failure in Percussion Drilling". *American Rock Mechanics Association.* ARMA/USRMS 05-819.

51. Katz, O., Reches, Z. and Roegiers, J-C. (2000). "Evaluation of Mechanical Rock Properties using a Schmidt Hammer". Technical Note. *International Journal of Rock Mechanics and mining science 37 (2000) 723-728*

52. Azar, J.J. and Samuel, G. R. (2007). "*Drilling Engineering*". TN871.2.A92 2007. PennWell Corporation.

53. Maurer, W. C. (1966). "The State of Rock Mechanics Knowledge in Drilling". *The 8th U.S. Symposium on Rock Mechanics (USRMS)*. ARMA 66-0355.

Appendix A 20*sim* Programming Codes for Rock Model

// Impact force profile generation code//

```
Parameters
        real hidden g= 0.05;
        real hidden Tr = 0.0001;
        real hidden Tf = 0.0001;
        real hidden P=50000.0;
        real hidden totalStroke = 0;
        real hidden startLevel = 0;

variables
        real hidden period;
        real hidden fu;
        real hidden offsetTime, modTime, divTime;
        real hidden stroke;
        real hidden duration;
        real hidden normalizedRegionTime;
        real hidden runningTime;
        integer hidden localProfileCounter;
        integer hidden region;
        integer hidden ProfileCounter;
        real hidden globalStrokeOffset;
        real hidden localStrokeOffset;
        // dll-variables
        real hidden dllInput;
        real hidden dllOutput[3];
initialequations
        fu = 0.0;
        offsetTime = 0.0;
        modTime = 0.0;
```

```
        region = 0;
        stroke = 1.0;
        duration = 1.0;
        dllInput = 0.0;
        dllOutput = 0.0;
        modTime = 0.0;
        divTime = 0.0;
        offsetTime = 0.0;
        globalStrokeOffset = 0.0;
        localStrokeOffset = 0.0;
        normalizedRegionTime = 1.0;
        runningTime = 0.0;
        ProfileCounter = 1;
        localProfileCounter = 1;
        position = startLevel;
    period= Tr+Tf+g;
code
            runningTime = time - offsetTime;
            modTime = runningTime mod period;
            divTime = runningTime div period;
            localProfileCounter = 1 + round(divTime);
                globalStrokeOffset = startLevel + divTime * totalStroke;
                // determine in which region we are
                if modTime < g then
                    region = 1;
                    normalizedRegionTime = modTime/g;
                else
                    if modTime < (Tr+g) then
                        region = 2;
                        normalizedRegionTime = ( modTime - g) / Tr;
                    else
```

```
                region = 3;
                normalizedRegionTime = ( modTime - Tr-g) / Tf;
        end;
end;
        switch(region)
                case 1 do
                dllInput = normalizedRegionTime;
        dllOutput =  dll('MotionProfiles.dll', 'ProfileFlat', dllInput);

                localStrokeOffset = 0;
                stroke = 0;
                duration = g;
                case 2 do
                dllInput = normalizedRegionTime;
        dllOutput = dll('MotionProfiles.dll', 'ProfileRamp', dllInput);

                localStrokeOffset = 0;
                stroke = P;
                duration = Tr;
                case 3 do
                dllInput = normalizedRegionTime;
        dllOutput = dll('MotionProfiles.dll', 'ProfileRamp', dllInput);
                localStrokeOffset = P;
                stroke = -P;
                duration = Tf;
        end;
        fu = dllOutput[1];
        position = (globalStrokeOffset + localStrokeOffset) + stroke * fu;
```

// Codes for Optimization Functions (SEI and PI)//

```
parameters
        real w1= 3.0;
        real w2= 2.0;
        real w3=0;
        real mxROP= 0.0830888;        // Insert the values
        real mxPavg= 7945.5;
        real mxBFavg= 180;
        real mxBFpk= 10;
variables
        real Pavg;
        real SEI;
equations
         Pavg=(int(P));
        Output=-(w1*ROP/mxROP)+
(w2*Pavg/mxPavg)+w3*(BFpk/mxBFpk)+w3*(BFavg/mxBFavg);
if ROP>0.00001 then
SEI= (Pavg/ROP);
else
SEI=0;
end;
```

// Codes for inductive element (I) or bit mass (m)//

```
parameters
        real i = 1.0;              // Input drill bit mass in kg
equations
        state = int(p.e);
        p.f = state / i;
```

// Codes for conductive element (C) or rock stiffness (k)//

```
parameters
        real k = 9.02e7;
```

```
        real Ks=1;
equations
        state = int(p.f);
        p.e = Ks*state * k;
```

// Codes for resistive element (R) or rock damping (b)//

```
parameters
        real b =1.34e3;
        real Kb=1;
equations
        p.e =Kb* b * p.f;
port1=p.e;
```

// Codes for resistive element (R) or threshold of dry friction element (D) //

```
parameters
        real global DV;              // Selected small velocity region
        real Fkin= 1453;             // Equal threshold force of dry friction element
        real FH= 1453;
variables
        real v;
        real Fslip;
        integer S;
        real Fo;
        real Fstick,x3,x4,x3old;
initialequations
        S = 1;
equations
        v = p.f;
        if abs(v) > DV then
                Fslip = Fkin*sign(v);
                S = 0;
```

```
        else
                Fslip = 0;
                S = 1;
        end;
        Fo = S*F;
        if abs(Fo) < FH then
                Fstick = Fo;
        else
                Fstick = FH*sign(Fo);
        end;
        p.e = Fstick + Fslip;
```

// Codes for inductive element (I) or small mass of rock cuttings (Mr)//

```
parameters
        real global DV;
        real m = 0.001;
variables
        real mo;
equations
        mo = int(p.e);
        if abs(mo) > m*DV then
                p.f = mo / m;
        else
                p.f = 0;
        end;
        mass = m;
```

Appendix B Sample Calculation for Physical Parameters Estimation

This section will show the details calculation to determine the physical parameters of Berea sandstone using Hsieh's equations [32] discussed in chapter 3. Mechanical properties of Berea sandstone are listed in Table B1.

Table B1 Mechanical Properties of Berea sandstone

C, MPa	E, GPa	ν	ρ, kg/m^3
66.6	15.2	0.37	2100

Effective contact area (A) can be calculated for a flat button bit having a button diameter of 0.6 in and total number of buttons of 17.

$$A = n\frac{\pi}{4}d^2 = 17.\frac{\pi}{4}(0.6)^2 = 4.8in^2 = 3.1x10^{-03}m^2 = 4.8\ \text{in}^2 = 3.1\text{x}10^{-03}\ \text{m}^2$$

Hence, Effective contact radius, $r = \sqrt{\frac{A}{\tau}} = \sqrt{\frac{3.1x10^{-03}}{\tau}} = 0.0314m$

Shear modulus of elasticity, $G = \frac{E}{2(1+\nu)} = \frac{15.2}{2(1+0.37)} = 5.547$ GPa

Now, dimensionless frequency $(a_o) = \omega r\sqrt{\frac{\rho}{G}}$ [32]. ω is circular frequency of the applied force. A frequency of 10Hz gives a value for a_o is 0.001. Reissner's displacement functions f_1 and f_2 are dependent on a_o. Corresponding to this value of a_o, f_1 and f_2 are 0.15 and 0.001 respectively [32]. The values of a_o, f_1 and f_2 are fixed

for the whole analysis as this value doesn't change too much for the entire frequency range of practical percussion drilling.

Threshold force of dry friction element, $= CA_e$ =66.6x10^6 x 3.1x10^{-03} =206.46 kN

Stiffness, k = $Gr\frac{f_1}{f_1^2 + f_2^2} = 5.547x10^9 x0.0314\frac{0.15}{0.15^2 + 0.001^2} = 1.16x10^9 N/m$

Damping coefficient,

$$b = \frac{r^2}{a_o}\sqrt{G\rho}\frac{f_2}{f_1^2 + f_2^2} = \frac{0.0314^2}{0.001}\sqrt{5.547x10^9 x2100}\frac{0.001}{0.001^2 + 0.15^2}$$
$$= 1.5x10^5 N.s/m$$

Appendix C Model Results (Tuned)-TerraTek Single Cutter Impact Test

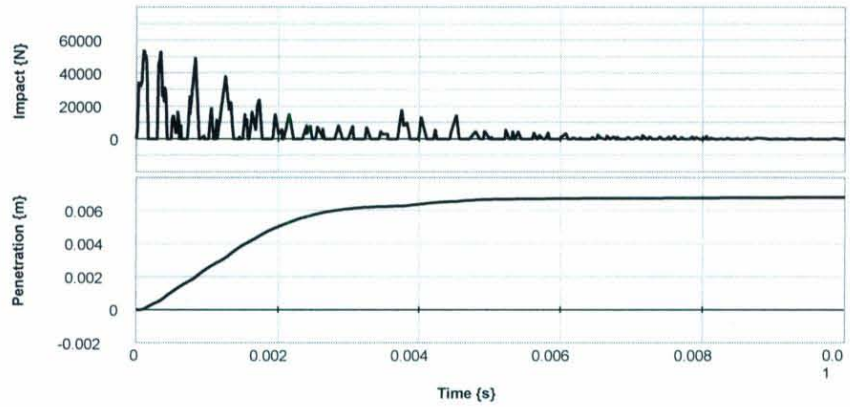

Figure C1 Model force and penetration results for Mancos shale at 0 psi

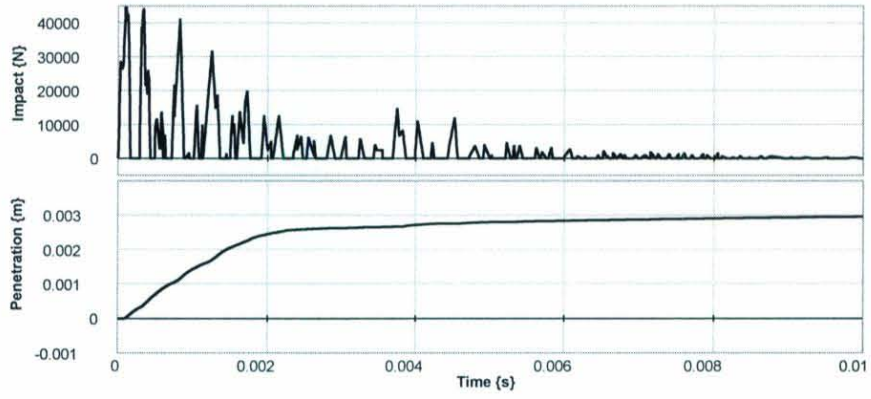

Figure C2 Model force and penetration results for Mancos shale at 3000 psi

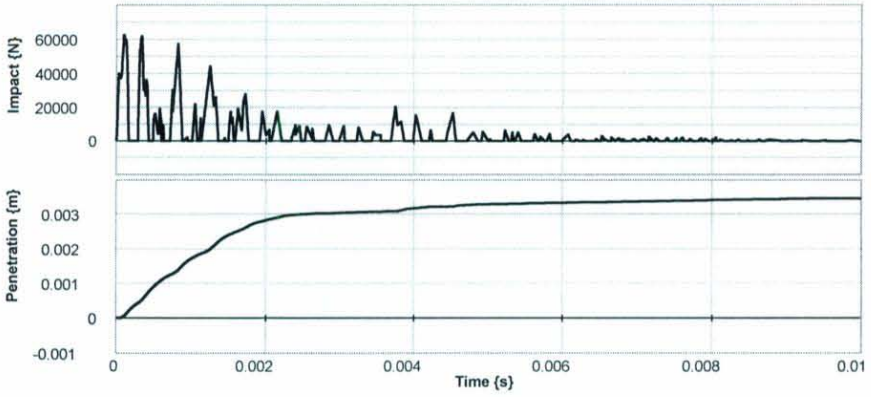

Figure C3 Model force and penetration results for Carthage marble at 0 psi

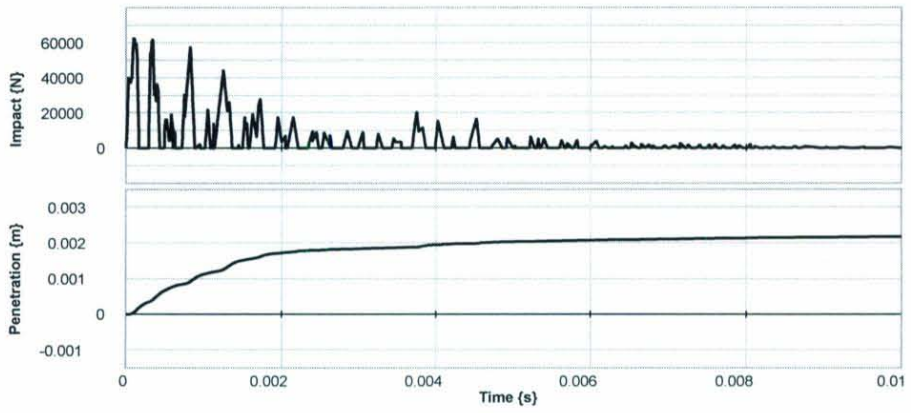

Figure C4 Model force and penetration results for Carthage marble at 500 psi

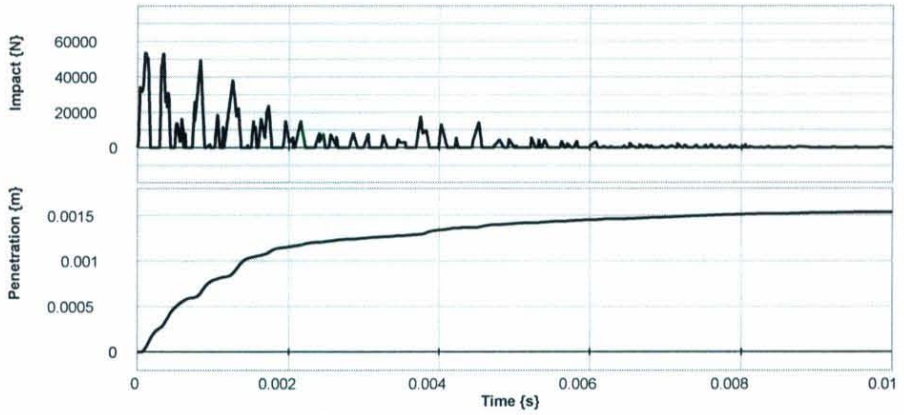

Figure C5 Model force and penetration results for Carthage marble at 1500 psi

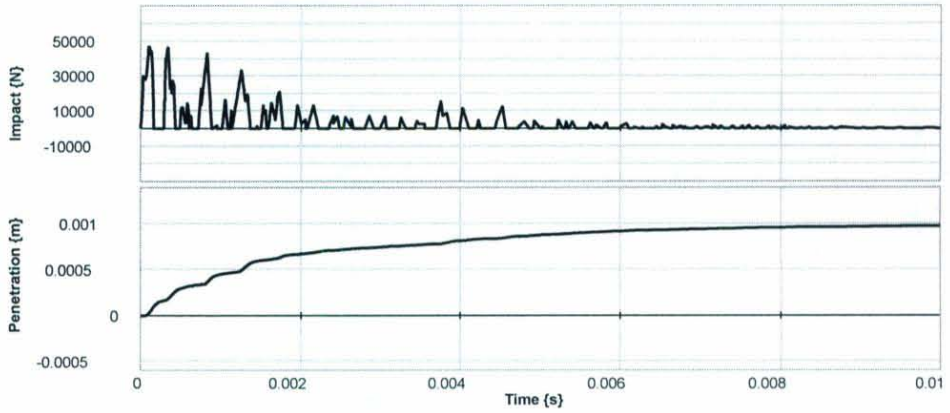

Figure C6 Model force and penetration results for Carthage marble at 3000 psi

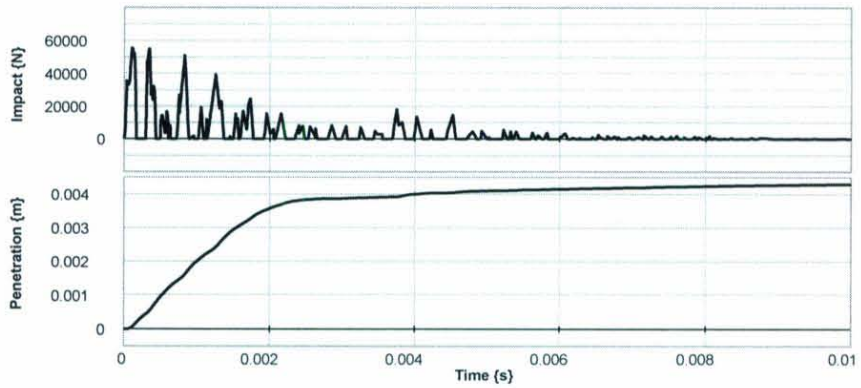

Figure C7 Model force and penetration results for Crab Orchard sandstone at 0 psi

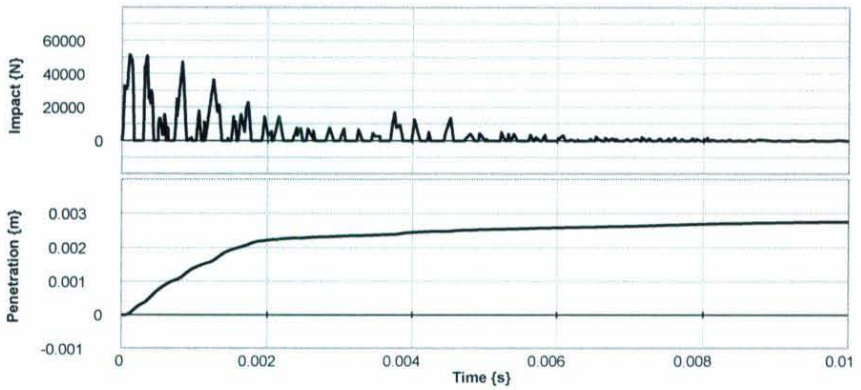

Figure C8 Model force and penetration results for Crab Orchard sandstone at 500 psi

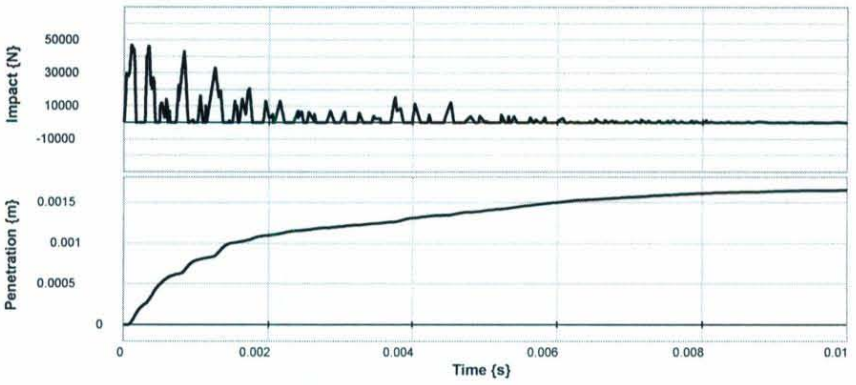

Figure C9 Model force and penetration results for Crab Orchard sandstone at 1500 psi

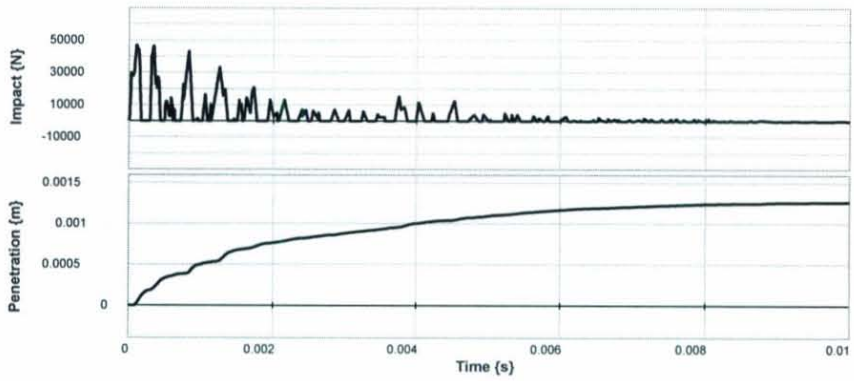

Figure C10 Model force and penetration results for Crab Orchard sandstone at 3000 psi

Appendix D Model Results (Tuned)-DRI Drop Test

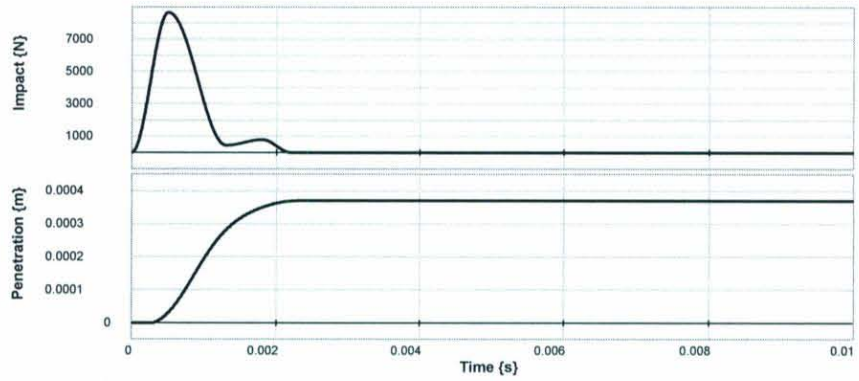

Figure D1 Model force and penetration results for a drop height of 39.68mm

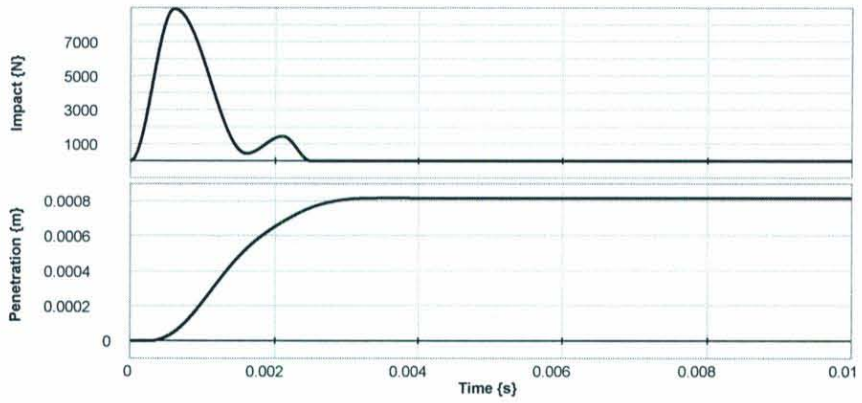

Figure D2 Model force and penetration results for a drop height of 69.85mm

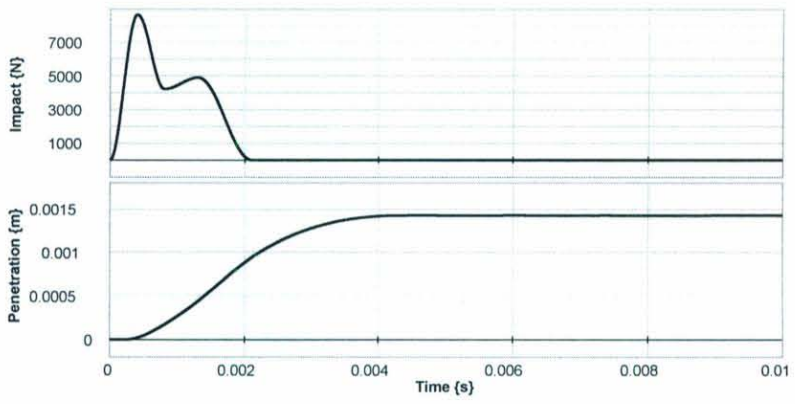

Figure D3 Model force and penetration results for a drop height of 114.3mm

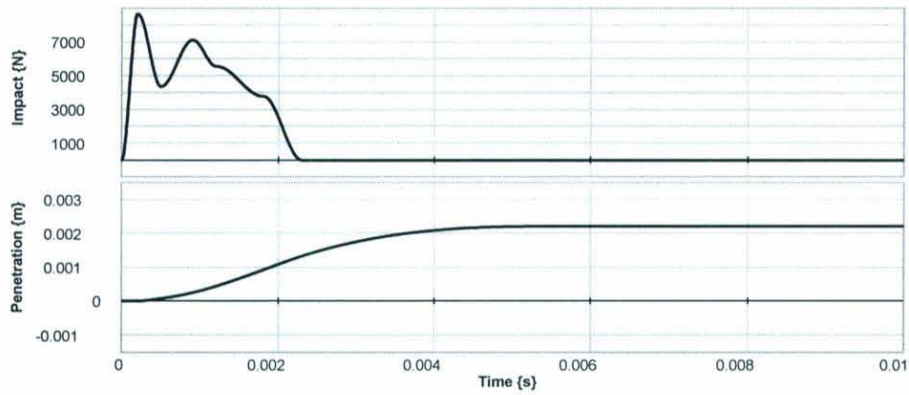

Figure D4 Model force and penetration results for a drop height of 190.5mm

PUBLICATION

Sazidy, M. S., Rideout, D. G., Butt, S. D. and Arvani, F. 2010. "Modeling Percussive Drilling Performance Using Simulated Visco-Elasto-Plastic Rock Medium". 44th US Rock Mechanics Symposium and 5th U.S.-Canada Rock Mechanics Symposium, ARMA 10-434.